


REVIEW

Open Access



Research Progress of Refractory High Entropy Alloys: A Review

Xiaochang Xie^{1,2}, Neng Li², Wei Liu², Shuai Huang², Xiaoyong He², Qiuying Yu^{2*} , Huaping Xiong^{2*}, Enhui Wang¹ and Xinmei Hou¹

Abstract

Owing to superior comprehensive performance than conventional superalloys at high temperature, refractory high entropy alloy (RHEA) is becoming a promising candidate for the next generation high-temperature material. Herein, contemporary aspects of corresponding development of RHEAs are reviewed to discuss various factors affecting the organization structure and service performance. It mainly covers alloying system and strengthening mechanism, the preparation method, plastic deformation and the related mechanism, as well as microstructure control by heat treatment. Firstly, the alloy systems and strengthening mechanism are introduced. This is followed by different preparation methods and the comparison of strengths and shortcomings based on different RHEAs. Then, hot deformation behavior and plastic deformation under different loadings are analyzed. Based on this, the influence of heat treatment on microstructures prior to and after the deformation is further summarized. Finally, some important research areas to be carried out in future are pointed out. This review will give a deep understanding of the effects of different factors on the service performance and provide scientific guide in designing RHEAs with improved performance.

Keywords: Refractory high entropy alloy, Preparation method, Strengthening, Plastic deformation, Heat treatment

1 Introduction

The requirement for higher temperature materials with superior performance is more stringent due to more and more complex and harsh service environment with the rapid development in the fields of aerospace, aircraft, nuclear reactors, transportation, chemistry, and other fields. For example, at present, nickel-based superalloy is prevalently used [1], but it is approaching the limits for improving operating temperature of turbine disk due to approaching design limits of alloy composition and serious difficulty to the manufacture of highly alloyed forgings [2, 3]. This is also true to those cast superalloys for turbine blades or vanes. High temperature ceramic [4], intermetallic [5], and Co-Re-based alloy [6] studied for substitutes for nickel-based superalloys, are incapable of

the requirement of turbine disk-blade/vane performance. Therefore, it is necessary to develop revolutionary new high-temperature structural materials.

High entropy alloy (HEA) is a subversive new concept of alloy design proposed by Yeh et al. [7] and Cantor et al. [8] in recent years. Different from traditional alloys with one or two dominating basic elements, such as nickel-based superalloy, titanium alloy, and so on, HEAs referred as multi-principal-element alloys, concentrated solid solution alloys, baseless alloys, or compositionally complex alloys, are composed of 5 or more elements in equiatomic, near equiatomic or unequi-atomic ratios, in which atomic percentage of each element varies from 5% to 35% [9]. Consequently, HEAs have unique effects including high entropy, lattice distortion, sluggish diffusion, and cocktail compared with traditional alloys [10–12]. This makes HEAs possess outstanding properties such as high hardness and strength, excellent thermal stability, high toughness, good ductility, excellent oxidation, wear and corrosion resistance [13–15], and so on,

*Correspondence: qiuyingyu@126.com; xionghuaping69@sina.com; xionghp69@163.com

² Beijing Institute of Aeronautical Materials, Beijing 100095, China
Full list of author information is available at the end of the article

providing a new choice for development of high-performance materials.

HEA consisting predominantly of refractory elements with high melting point such as Nb, V, Zr, Ta, Hf, Mo, and W, is generally considered as refractory high entropy alloy (RHEA). RHEA first proposed by Senkov et al. in 2010 [16], exhibiting typical characteristics of HEAs and better high-temperature performance than conventional Inconel 718 superalloy, has been recently emphasized as the next generation high temperature structural materials due to the potential to replace nickel-based superalloy except high costs [17, 18], and researches on RHEAs have become a hot-spot due to their possible high-temperature applications.

In this paper, the important research progress of RHEAs are reviewed and will be focused on alloy systems and strengthening mechanism, preparation method, plastic deformation and related mechanism, microstructure control via heat treatment. Lots of RHEAs systems are discussed, and significant research results have been obtained, and finally the current challenges and future research work are addressed.

2 Progress of Refractory High Entropy Alloys

2.1 Refractory High Entropy Alloy Systems and Strengthening Mechanism

Since alloy softening generally occurs at temperatures higher than $0.5T_m - 0.6T_m$, where T_m is melting point, RHEAs featuring high melting points can exhibit higher strength at elevated temperatures (>800 °C) compared with widely used nickel-based superalloys such as Inconel 718 and Haynes 230 [19–22], which enables RHEAs to be very promising alternatives for high-temperature applications. Nevertheless, most RHEAs exhibit lower ductility at room temperature and/or poor phase stability at high temperatures [23–26].

Single-phase RHEAs are usually more ductile than multi-phase RHEAs and offer good high-temperature phase stability [27], and therefore high strength. However, it is still challenging to simultaneously achieve good RT ductility and high strength and good phase stability at high temperatures. For example, WNbMoTa alloy which is one of the most classical RHEAs initially developed by Senkov et al. exhibits a single-phase structure and the exceptionally high yield strength (405 MPa) at 1600 °C, but it has only 2.1% fracture strain at room temperature [19]. Until now, only TiZrHf alloyed with Ta, Nb, and Nb-Ta reveals single-phase structures at RT and tensile fracture strains $\sim 15\%$ – 30% that are comparable to Ni-based superalloys, but these alloys are relatively weak above 1000 °C and show poor phase stability at high/medium temperatures [28].

In recent years, intense efforts have been devoted to improving mechanical properties of RHEAs for various

potential applications. The development directions focused on the following two points: ① Alloying; ② Addition of secondary ceramic particles.

2.1.1 Alloying Effect

It is well known that alloying is an effective method to improve mechanical properties of alloys [29]. For the RHEAs, it is necessary to design single-phase disordered solid solution RHEAs and to adjust their properties via alloying for the improvement of high-temperature strength and RT ductility.

Wang et al. [30] explored novel $V_x\text{NbMoTa}$ RHEAs with vanadium concentrations of 0–25 at.%. $V_x\text{NbMoTa}$ RHEAs exhibit a single body-centered cubic (BCC) structure with unprecedented phase stability at a wide temperature range from solidus down to 350 °C. The grain structure of $V_x\text{NbMoTa}$ can be substantially refined when increasing the V concentration since higher V contents induce stronger solution effects which contribute to higher growth restriction factors. Equimolar VNbMoTa exhibits the yield strength of 811 MPa at 1000 °C, which is superior to most RHEAs reported by far, and this alloy also shows excellent room temperature ductility with the fracture strain $>25\%$ and no strain-softening at high temperature, indicating evident advantages compared with many popular RHEAs, as shown in Figure 1.

Han et al. [31] reported that the addition of Ti element in the TiNbMoTaW and TiVNbMoTaW RHEAs was beneficial to the strength and the compressive ductility of the refractory HEAs at room-temperature. The RHEAs possess single BCC phase structure, and could sustain the phase structure even after annealing at 1200 °C for 24 h. The room-temperature yield strengths of the TiNbMoTaW and TiVNbMoTaW HEAs are 1343 and 1515 MPa, respectively. Meanwhile, their compressive plastic strains at room temperature are above 10%. Their yield strengths are as high as ~ 586 and ~ 659 MPa at 1200 °C, respectively. The effects of Ti additions on the mechanical properties of these HEAs can be interpreted in terms of a solid solution hardening model. The engineering stress-strain curves of the TiNbMoTaW and TiVNbTaMoW HEAs at room temperature and elevated temperatures are shown in Figure 2 and the mechanical properties of both alloys are given in Table 1 [31, 32].

Ge et al. [33] investigated the effects of Al element addition on the mechanical properties of $Al_x\text{MoNbTaTiV}$ RHEAs, as shown in Figure 3. As the Al content increases, the lattice constant decreased from 3.211 to 3.199 Å. The yield strength increases from 1228 to 1391 MPa, the hardness increases from 421 to 575 HV. The solid solution strengthening mechanism of Al in the refractory high entropy alloy depends on its chemical interaction and electronic interaction. At room temperature, the

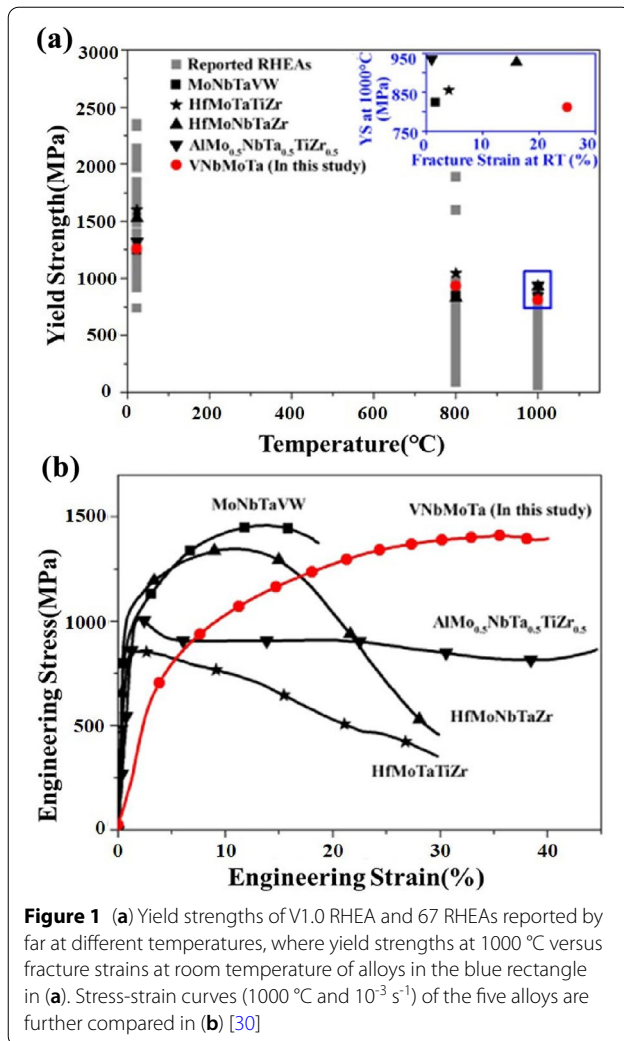


Figure 1 (a) Yield strengths of V1.0 RHEA and 67 RHEAs reported by far at different temperatures, where yield strengths at 1000 °C versus fracture strains at room temperature of alloys in the blue rectangle in (a). Stress-strain curves (1000 °C and 10^{-3} s⁻¹) of the five alloys are further compared in (b) [30]

addition of Al enhanced the dynamic aging effects in low concentration, but the effects became weaker with the increase of Al content. At 500 °C, higher Al concentration led to stronger serrated flow.

NbMoTaW RHEA has shown great potential applications for high temperature components due to its high temperature mechanical strength. However, the brittleness at room temperature hinders its engineering application and further development. To solve this problem, refractory alloying elements with melting temperatures over 1850 °C, i.e., Cr, Zr, V, Hf, and Re, were ideal options to enhance the mechanical performance. Tong et al. [34] researched on the effects of refractory alloying elements on the strength and ductility of NbMoTaW RHEA, as shown in Figure 4. Most of alloying elements ($x = \text{Cr, Zr, V, Hf}$ and Re) enhanced the strength of NbMoTaW RHEA, while only Zr-alloying improved both the strength and ductility simultaneously, as shown in

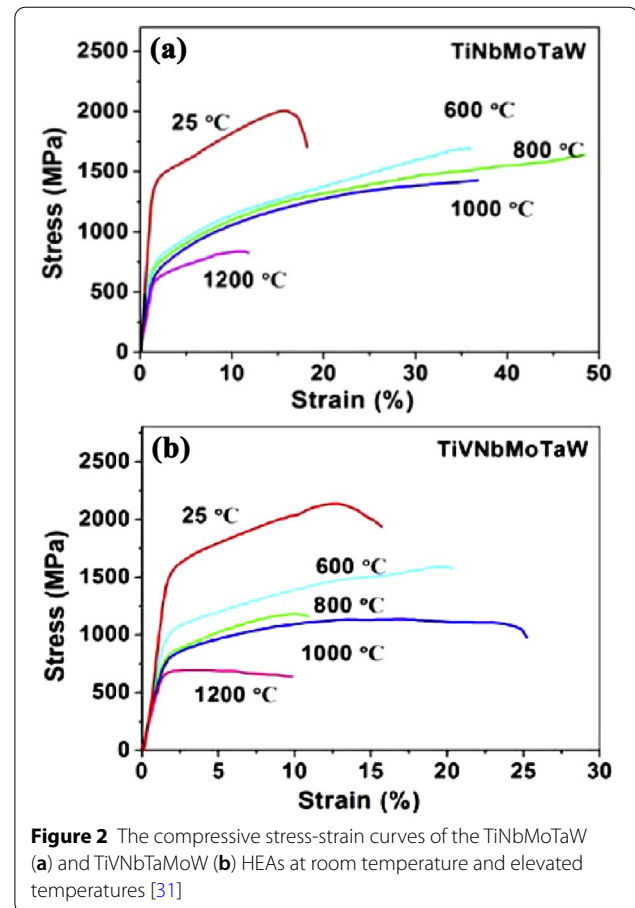


Figure 2 The compressive stress-strain curves of the TiNbMoTaW (a) and TiVNbMoTaW (b) HEAs at room temperature and elevated temperatures [31]

Table 2. The strengthening mechanism was well analyzed based on electronic structures. The formation of partial Zr-Zr metallic bonds effectively improved the strength and ductility of NbMoTaW RHEA from the perspective of experiments and theoretical predictions.

2.1.2 Addition of Secondary Ceramic Particles

It is well known that addition of secondary ceramic particles, such as carbides, nitrides, or silicides, is an effective method to improve the strength of metallic materials [35, 36]. Based on this design strategy, some RHEA-based composites were developed.

Long et al. [37] investigated the NbMoTaWVCr RHEA with secondary ceramic particle reinforcements. The sample sintered at 1500 °C exhibited a multi-phase microstructure with 7.7% Laves phase and 6.2% Ta₂VO₆ particles distributed in equiaxed BCC matrix with the average grain size of 1.24 μm, as shown in Figure 5. The fine grain size and homogeneous dispersion of tiny particles enabled the sintered HEA to possess both high strength and fair plasticity. The yield strength (σ_y), plastic strain (ϵ_p) and Vickers hardness (HV) of this HEA

Table 1 Yield strength, peak strength and plastic strain at different temperatures of the TiNbMoTaW, NbMoTaW, TiVNbMoTaW and VNbMoTaW HEAs [31, 32]

Alloy/properties	TiNbMo-TaW	NbMo-TaW	TiVNb-MoTaW	VNbMo-TaW	
1	$\sigma_{0.2}$ (MPa)	1343	1058	1515	1246
	σ_p (MPa)	2005	1211	2135	1270
	ε_p (%)	14.1	2.6	10.6	1.7
2	$\sigma_{0.2}$ (MPa)	689	561	973	862
	σ_p (MPa)	1681	–	1590	1597
	ε_p (%)	35.4	>20	18.8	13
3	$\sigma_{0.2}$ (MPa)	674	552	791.3	846
	σ_p (MPa)	1618	–	1180	1536
	ε_p (%)	46.6	>20	9.4	16
4	$\sigma_{0.2}$ (MPa)	620	548	752.8	842
	σ_p (MPa)	1426	1008	1105	1454
	ε_p (%)	35.5	>20	23.7	19
5	$\sigma_{0.2}$ (MPa)	586	506	659	735
	σ_p (MPa)	814	803	696	943
	ε_p (%)	10.2	>20	8.4	8
1400°C	$\sigma_{0.2}$ (MPa)	–	421	–	656
	σ_p (MPa)	–	–	–	–
	ε_p (%)	–	>40	–	18
1600°C	$\sigma_{0.2}$ (MPa)	–	405	–	477
	σ_p (MPa)	–	–	–	–
	ε_p (%)	–	>40	–	13

arrived at 3416 MPa, 5.3% and 9908 MPa, respectively. This ultra-high strength and hardness dramatically exceeded other cast or sintered refractory HEAs. The main strengthening mechanisms in the sintered NbMo-TaWVCr are interstitial solid solution strengthening, grain boundary strengthening and inherent solid solution strengthening.

Lv et al. [38] prepared a multiple nonmetallic atoms co-doped CrMoNbWTi RHEA by mechanical alloying (MA) and spark plasma sintering (SPS). The as-sintered RHEA co-doped with C, N, and O exhibited ultra-high strength and hardness of 4345 MPa and 11.88 GPa, respectively. The microstructural observations indicated that both N and O were completely reacted with the refractory metallic elements to in-situ generate massive dispersed refractory compounds of (Nb,Ti)N and Ti_2O_3 , while C was mainly dissolved in the BCC solid-solution phase. The microstructural analysis results indicated that the CrMoNbWTi-CNO RHEA had a fine and homogeneous microstructure without obvious aggregation and grain coarsening, as shown in Figure 6. The excellent mechanical properties were attributed to not only traditional solid solution, grain boundary, Orowan strengthening mechanisms, but also the additional C interstitial strengthening

and intergranular refractory compounds of (Nb,Ti)N and Ti_2O_3 , as shown in Figure 7.

In the reported literatures on particles reinforced RHEAs, Lv et al. [39] fabricated a novel CrMoNbWTi-C RHEA co-strengthened by fine-grained intermetallics (IM) and ultra-high temperature carbides (UHTC) particles by MA and hot-press sintering (HPS), as shown in Figure 8. During the MA process, a supersaturated BCC solid solution was formed. Subsequently, during HPS, the IM of Cr_2Nb and UHTC of (Ti,Nb)C were precipitated from the BCC solid solution. The as-sintered RHEA with multiphase structure exhibited an ultra-high fracture strength of 3094 MPa and superior hardness of 8.26 GPa, respectively. The as-sintered sample had a fine and homogeneous microstructure without obvious aggregation and grain coarsening. The three different phases were well dispersed with each other. Therefore, besides the traditional grain boundary strengthening and solid solution strengthening mechanisms, the hard and refractory Cr_2Nb and (Ti,Nb)C phases co-strengthening also plays a vital role in the enhancement of strength and hardness.

Kang et al. [40] investigated the $Nb_{42}Mo_{20}Ti_{13}Cr_{12}V_{12}Ta_1$, a novel RHEA enriched with niobium (Nb). The microstructure of the bulk RHEA

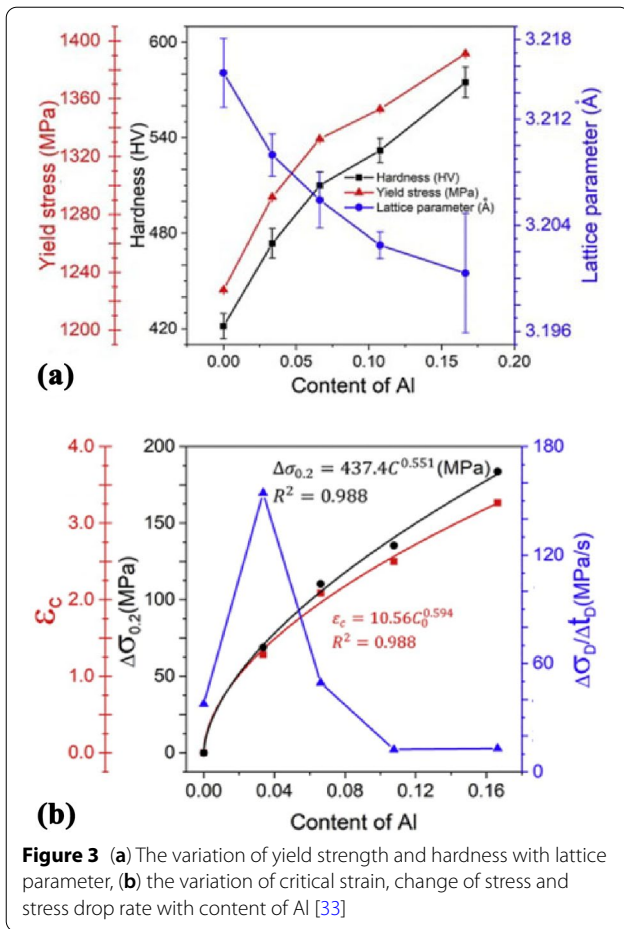


Figure 3 (a) The variation of yield strength and hardness with lattice parameter, (b) the variation of critical strain, change of stress and stress drop rate with content of Al [33]

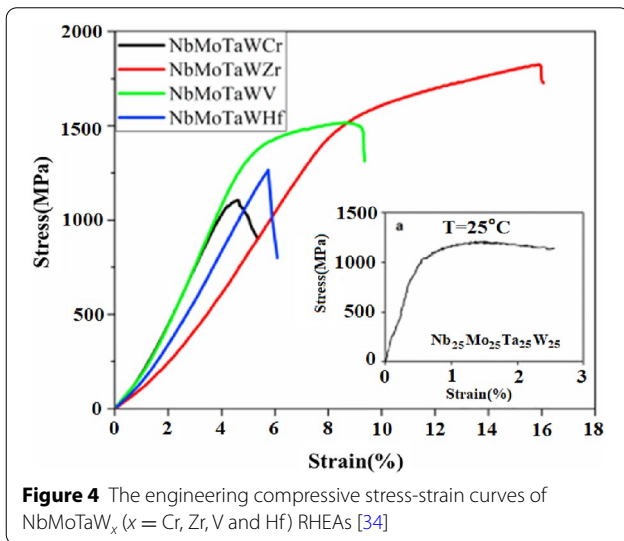


Figure 4 The engineering compressive stress-strain curves of NbMoTaW_x (x = Cr, Zr, V and Hf) RHEAs [34]

Table 2 Compressive properties of NbMoTaW_x (x = Cr, Zr, V, Hf and Re) RHEAs [34]

Alloys	Yield stress (MPa)	Peak stress (MPa)	Peak strain (%)
NbMoTaW	1058	1211	<3
NbMoTaWCr	1056	1104	4.6
NbMoTaWZr	1480	1822	15.9
NbMoTaWV	1460	1520	8.8
NbMoTaWHf	1252	1252	5.7
NbMoTaWRe	1062	1147	4.2

the short sintering time, and the impedance of the grain growth caused by the dispersoids led to the formation of nano-sized grains, in spite of the high sintering temperature of 1200 °C. With the nano-sized TiC dispersoids dispersed homogeneously throughout the alloy, the bulk Nb₄₂Mo₂₀Ti₁₃Cr₁₂V₁₂Ta₁ RHEA exhibits a compressive yield strength of 2680 MPa, a maximum strength of 3896 MPa, and a Vickers hardness of 741 HV. These excellent mechanical properties were attributed to the extreme grain refinement and dispersion strengthening caused by the TiC that was formed in-situ, and the lattice distortion effects induced by the interstitial carbon and differences between the atomic sizes of each alloying element.

2.2 Preparation Method

The preparation of RHEAs is a great challenge due to high melting point of refractory elements [41]. Processing routes can be broadly classified into four groups, namely, melting-casting, mechanical alloying, deposition, and additive manufacturing. Melting and casting has been used to produce HEAs in the shape of rods, bars, and ribbons. The most popular melt processing techniques are vacuum arc melting (VAM), vacuum induction melting (VIM), and magnetic levitation melting (MLM). MA followed by sintering has been the major solid-state processing route to produce sintered products. Sputtering, plasma nitriding and cladding are the surface modification techniques used to produce thin films and thick layers of HEAs on various substrates. Additive manufacturing (AM) has the characteristics of accurate manufacturing and rapid solidification, which can ensure microstructure uniformity better than traditional preparation processes. Furthermore, AM conducive to microstructure refinement is helpful to improve mechanical properties of high entropy alloy.

formed a single BCC matrix with in-situ-formed carbide dispersoids, as shown in Figure 9. The combination of the effect of the severe deformations caused by the milling,

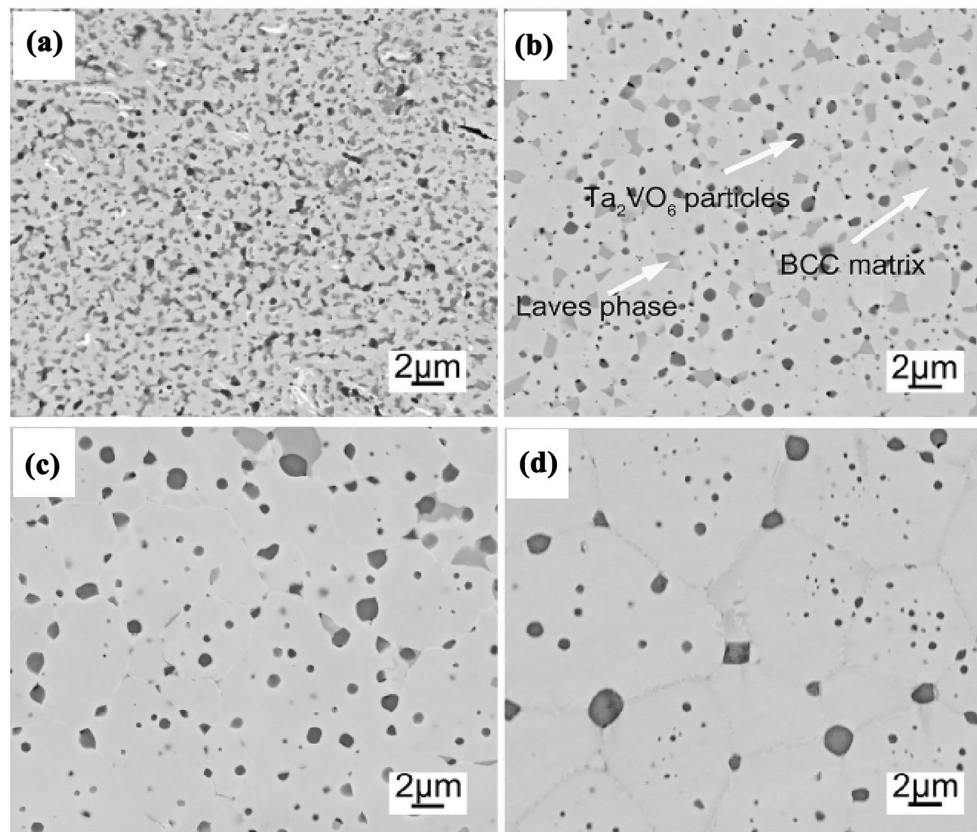


Figure 5 SEM backscattered electron images of the bulk NbMoTaWVCr HEA alloys sintered at different temperatures: (a) 1400, (b) 1500, (c) 1600 and (d) 1700 [37]

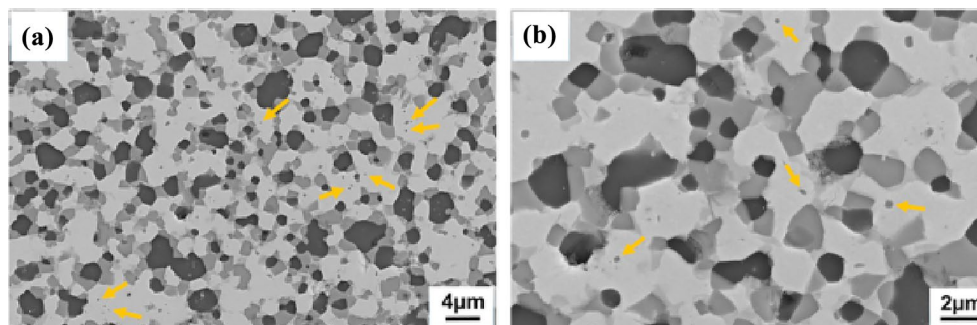


Figure 6 Microstructures of the as-sintered CrMoNbWTi-CNO RHEA: SEM micrographs at (a) low magnification and (b) high magnification [38]

2.2.1 Melting-casting

The mixing of liquid alloying elements by arc, induction, or laser is main methods for RHEAs preparation. VAM is the earliest and most widely utilized [42, 43], using the arc generated between the two electrodes to melt the material, as shown in Figure 10. The earliest series of RHEAs, such as $\text{Nb}_{25}\text{Mo}_{25}\text{Ta}_{25}\text{W}_{25}$ and $\text{V}_{20}\text{Nb}_{20}\text{Mo}_{20}\text{Ta}_{20}\text{W}_{20}$

proposed by Senkov et al. [16], were prepared by VAM, with room-temperature yield strength of 1058 MPa and 1246 MPa, respectively. Couzinié et al. [44] successfully produced equimolar TiZrHfNbTa RHEA using arc melting and induction techniques. Yang et al. [45] prepared HfNbTaTiZr RHEA using VAM and its yield strength were 1597 MPa at room temperature and 356 MPa at

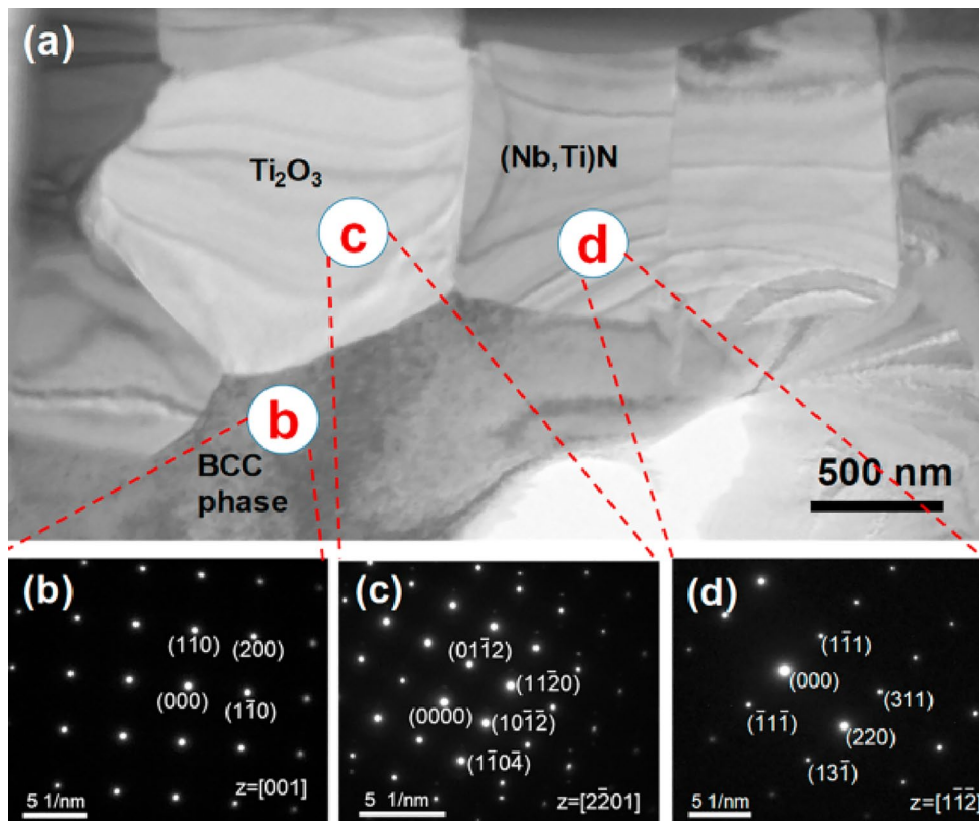


Figure 7 TEM images of CrMoNbWTi-CNO HEA: (a) bright-field image, diffraction patterns of (b) BCC matrix phase along [001] zone axis, (c) Ti_2O_3 phase along [2201] zone axis, (d) (Nb,Ti)N phase along [109] zone axis [38]

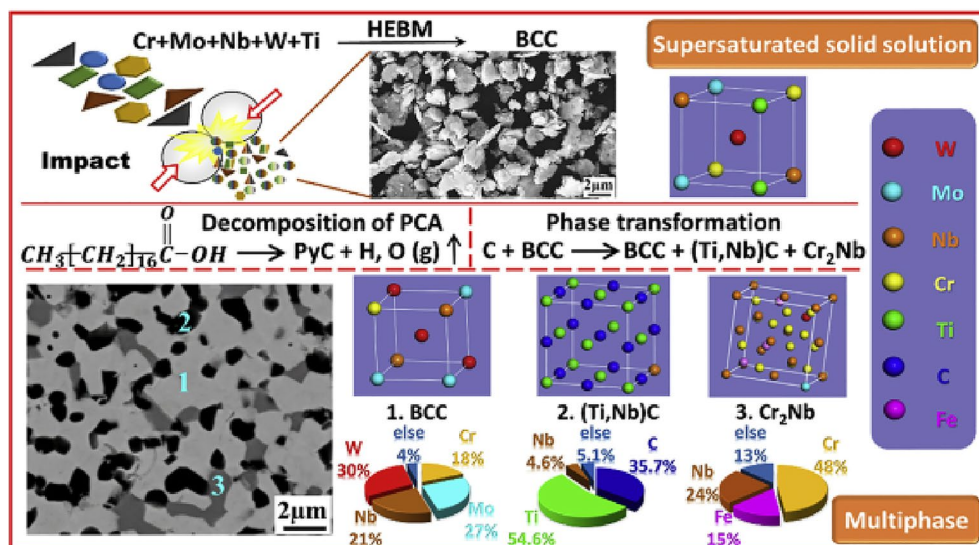


Figure 8 Schematic diagram of the phase evolution during hot-press sintering: The single BCC supersaturated solid solution transformed to multi-phases consisting of BCC, (Ti,Nb)C and Cr_2Nb . The conceivable crystal structure of each phase was shown by the illustrations of atomic location [39]

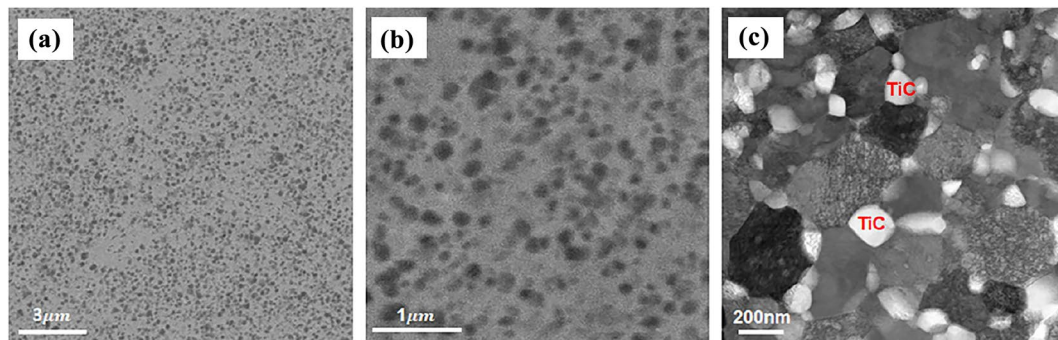


Figure 9 Scanning electron microscopy image of the bulk $\text{Nb}_{42}\text{Mo}_{20}\text{Ti}_{13}\text{Cr}_{12}\text{V}_{12}\text{Ta}_1$ RHEA after spark plasma sintering: (a) Low magnification, (b) High magnification, (c) Scanning transmission electron microscopy image of the bulk RHEA [40]

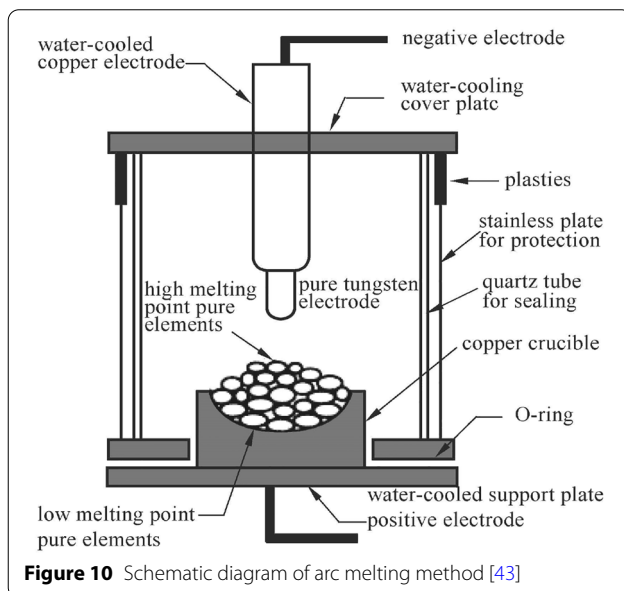


Figure 10 Schematic diagram of arc melting method [43]

1200 °C. Qiao et al. [46] prepared $\text{Ti}_2\text{ZrHf}_{0.5}\text{VNb}_x$ ($x = 0, 0.25, 0.5, 0.75, 1.0$) RHEA with BCC structure by VAM. Yu et al. [47] prepared $\text{Al}_a\text{Mo}_b\text{Nb}_c\text{Ta}_d\text{TiZr}$ ($a = 1.5, 0.5, 0.25; b = 0.5, 0.25, 0; c = 0.5, 0; d = 0.5, 0.75, 1$) by a nan-consumable vacuum arc melting. VAM is a melting technique by using an eddy current generated during electromagnetic induction. Wang et al. [48] used this method to prepare HfNbTaTiZrW and HfNbTaTiZrMoW RHEAs, and studied microstructure, and the contributions of Mo and W to high-temperature performance of the two alloys.

MLM is a new melting technology by using electromagnetic force to suspend raw materials in vacuum and to act simultaneously on metal liquid by electromagnetic heating and stirring. This technology has been widely used in recent years due to its low pollution, high

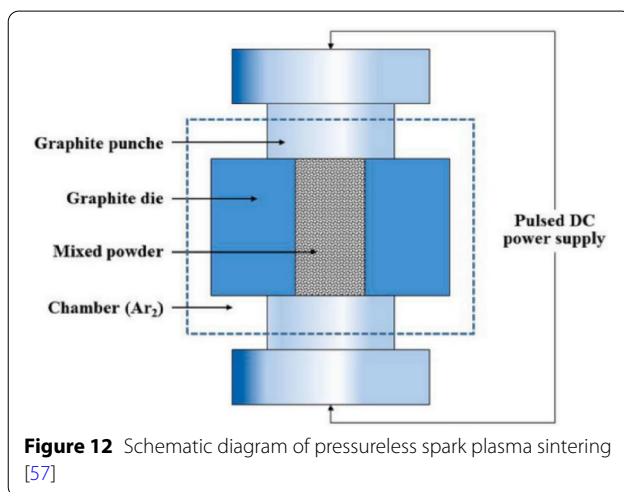
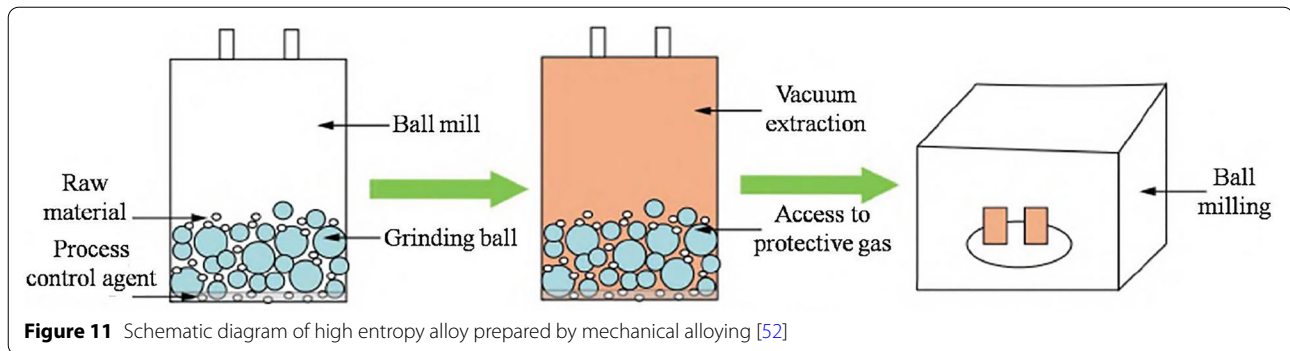
melting temperature, uniform composition and large size samples. Yu et al. [49] successfully prepared AlCoCrFeNiSiYHf HEA using MLM, and studied the influence of heat treatment at 1200 °C on alloy microstructure and mechanical properties.

However, significant disadvantages in liquid mixing of melting also occur in the melting-casting technique. Firstly, differences in the melting temperatures of different elements can lead to significant elemental segregation. Secondly, while segregation can be alleviated by increasing solidification rate, shrinkage cavities and residual stresses occur in the quenching of RHEAs. Consequently, rapid solidification poses difficulties for the preparation of large-scale RHEAs with uniform microstructures [50]. Moreover, solidification defects such as shrinkage cavities and pores are also generated in the castings [51]. Therefore, the development of RHEAs is mainly restricted by the above problems.

2.2.2 Mechanical Alloying

As an important preparation method of solid powder, MA has been widely used for the preparation of RHEAs. The RHEA powders are obtained through the preparation of element powder according to composition proportion, mechanical mixing evenly with high-energy ball grinding, and repeated cold welding, crushing and rewelding of powder particles [52], as shown in Figure 11. Afterwards, the bulk material can be prepared by thermal isostatic sintering (HIP) or SPS following the obtained alloy powders pressed in the mold.

MA is a rapid prototyping process with low energy consumption and high material utilization. The RHEAs samples prepared by MA have many advantages, including uniform and ultrafine microstructure, lower processing temperature, larger bulk volume, and better performance. MA process is also suitable for manufacturing RHEA



components for high temperature applications. And MA contributes to the formation of fine, uniform in-situ dispersions further strengthening RHEAs [40]. Waseem et al. [53] prepared $W_xTaTiVCr$ RHEAs with in-situ TiC and their derived alloys using MA. Guo et al. [54] synthesized a ductile and strong single-phase NbTaTiV RHEA by MA.

High-energy ball milling and subsequent powder consolidation such as SPS and hot pressing are important in the preparation of MA. Kang et al. [55] fabricated a MoNbTaTiV RHEA with ultra-fine grains and homogeneous microstructure by MA and SPS. Through appropriate sintering procedures, bulk materials or machined parts can be produced with desired shape, microstructure and properties [56]. In addition, pressureless SPS is an improved method suitable for rapid preparation of porous materials. A related study used pressureless SPS to prepare porous MoNbTaW RHEA with fine grains and easy pulverization into powder, as shown in Figure 12[57].

However, elemental contamination including Fe from powder balls and vessel walls and interstitial O, C, or N in the lattice from environmental and process control

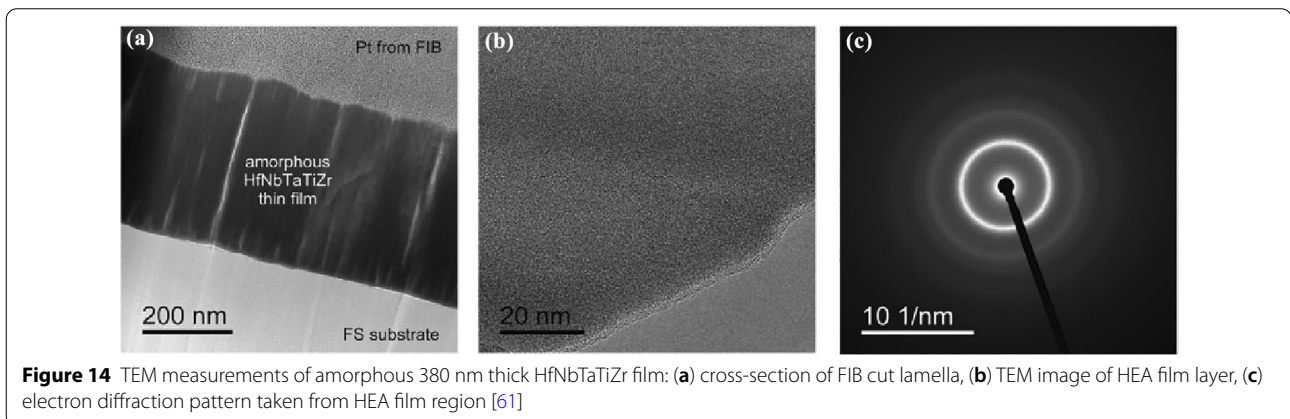
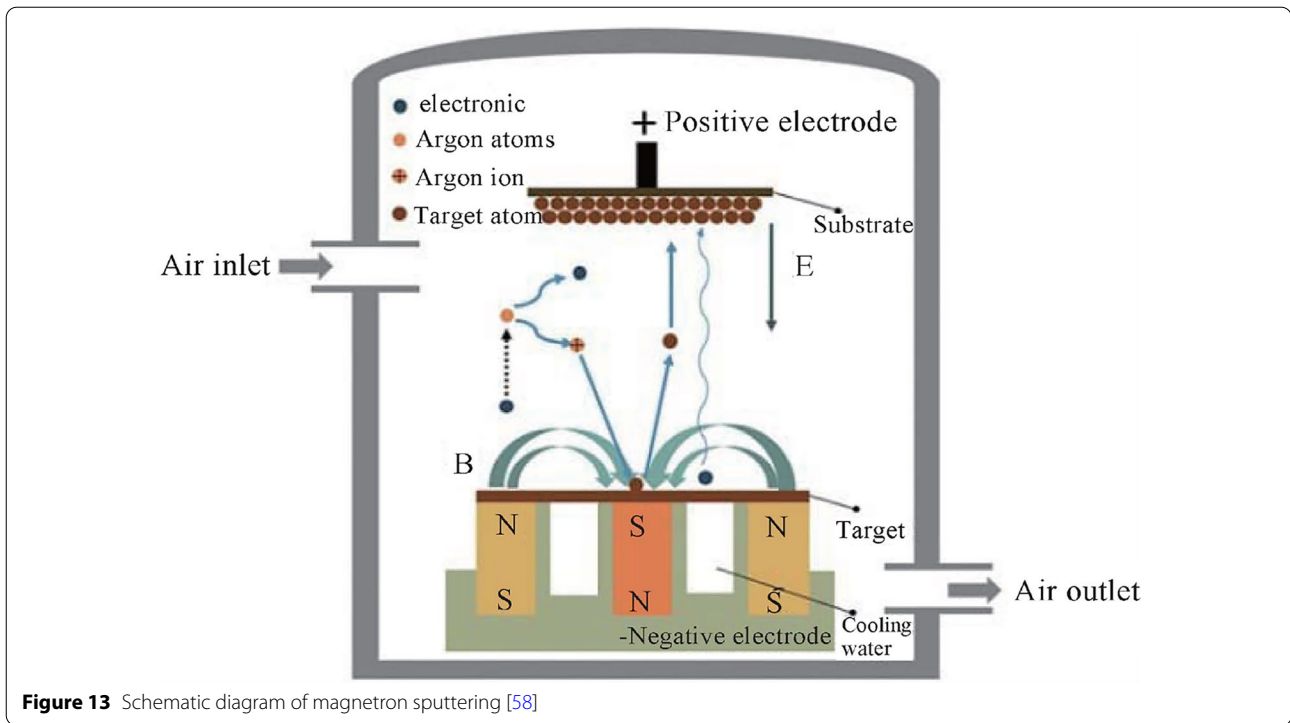
agents during MA, is a limiting factor of this preparation method.

2.2.3 Deposition Techniques

Gas process preparation methods for RHEA coatings or films present mainly include magnetron sputtering (MS), pulse laser deposition (PLD) and vapor deposition.

MS is a process of depositing molten metal droplets on a target in a specific atmosphere through a magnetic field to form a thin film, as shown in Figure 13, which can significantly enhance wear, corrosion and high-temperature resistance of the parts. Although the disadvantages including lower target utilization and difficult preparation of magnetic materials exist [58–60], MS has become one of the most commonly used methods due to its high efficiency and low cost among thin-films RHEA coating preparation methods. Kao et al. [60] fabricated $(TaNbSiZrCr)_x$ RHEA thin films using MS in a mixed atmosphere of Ar and C_2H_2 . Hruška et al. [61] deposited two HfNbTaTiZr RHEA films with thicknesses of 380 nm and 1650 nm on fused silica substrates by DC MS at room temperature, and found hard to avoid oxygen infiltration into HfNbTaTiZr films containing nanoscale open volumes favorable for hydrogen absorption, as shown in Figure 14. Chen et al. [62] prepared VAlTiCrMo and $(VAlTiCrMo)_xN_x$ RHEA thin films by MS, and the results showed that nitrogen significantly improved the hardness, elastic modulus and corrosion resistance of the coating.

PLD is similar to MS except bombardment energy source of a pulsed laser, and it exhibits higher deposition efficiency and no restrictions on deposition temperature and target species compared to MS. Dehestani et al. deposited FeCoNiMoW HEA coating and performed phase, elemental, and morphological evaluations to confirm the formation of alloy coatings with high entropy. The correlation between microhardness, magnetic, wear, and corrosion properties and



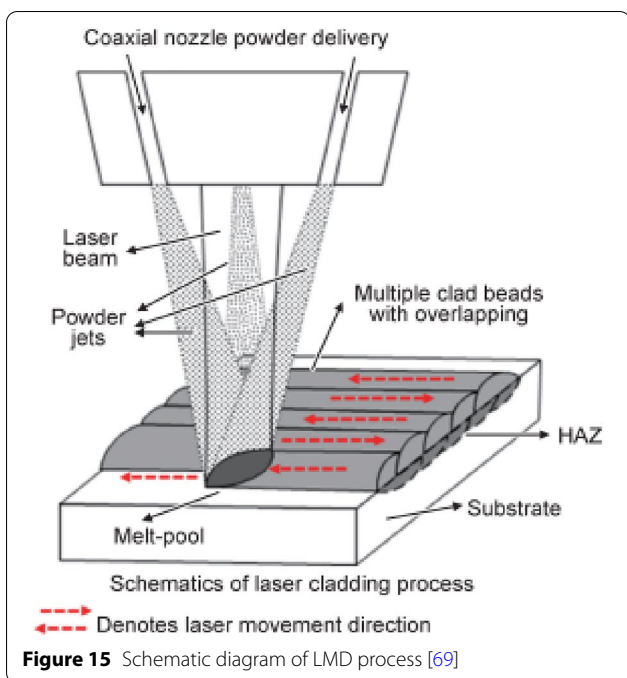
microstructure evolution was also investigated [63]. The PLD method is unable to prepare large size materials and has low preparation efficiency.

Electron beam evaporation is an evaporation coating technology, which uses the energy generated by the electron beam to evaporate the substrate and then condenses on the substrate. Electron beam evaporation is mostly used in the semiconductor preparation industry. Due to the large energy generated by the electron beam, it has the characteristics of evaporation of high melting point materials. Tao et al. [64] used this method to prepare a AlCrTiNbMo HEA coating on the Ti600 substrate surface greatly improved the low surface hardness and wear

resistance of Ti600 alloy via microstructure evaluation and hardness and wear resistance tests. The surface of the coating usually is quiet uniform, dense and smooth by electron beam evaporation method, but it is also expensive and difficult to control the coating quality.

2.2.4 Additive Manufacturing

Recently, AM as the preferred alternative to traditional manufacturing techniques, has been paid much attention. AM is a process of incrementally manufacturing materials layer by layer using 3D model data. Many advantages including the manufacture of complex structural parts and using difficult-to-machine materials (e.g., Ta, W, Mo,

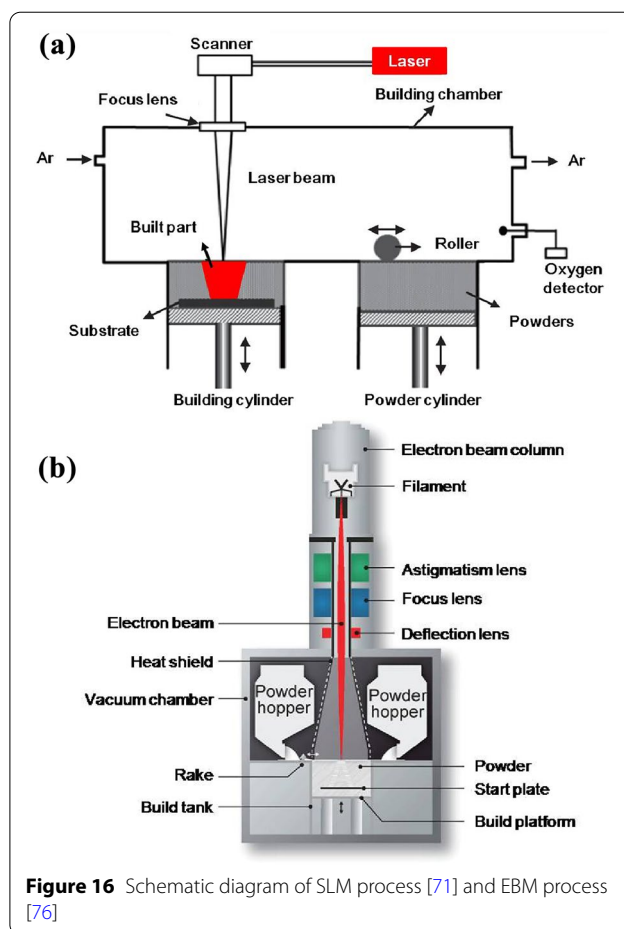


Nb, etc.) to manufacture parts are exhibited in AM compared with traditional processes. The process has higher design freedom and higher heating or cooling rates. In addition, AM enables functional hierarchical customization of the composition of manufacturing layers [65, 66].

The AM preparation methods mainly include direct energy deposition (DED) technology represented by laser melting deposition (LMD), direct laser deposition (DLD), laser cladding (LC), and powder bed fusion (PBF) technology represented by selective laser melting (SLM) and electron beam melting (EBM) [67, 68].

In the LMD process, powder particles were carried out by protective gas and concentrated on forming platform through the nozzle, and the laser beam was used to form a molten pool at the focal point. This process is repeated for each layer to eventually form a layer-by-layer deposition component [69, 70], as shown in Figure 15. Closed processing environment is not required due to inert gas blowing with LMD technology, leading to no limits on the size of parts. In-situ alloying can be achieved by LMD process with the whole variety of element powder delivered separately with multi-nozzle equipment. Moreover, high-throughput screening for gradient HEA can also be realized based on LMD by controlling the powder delivery rate during processing.

SLM is another typical AM process based on PBF technology that powders are spread onto a substrate and selected areas of each layer are scanned by high-energy laser beams to completely melt metal powders in the current area [71–75], as shown in Figure 16(a). After



processing one layer, molding platform drops a layer of height, and then laser scans continually to the next layer of powders, and finally forming parts. Highest molding precision can be exhibited in the SLM. Complex-shape parts can be directly formed by 3D model, without mold and subsequent machining.

EBM is basically similar to SLM process except the difference of heat sources, as shown in Figure 16(b) [76]. Compared with SLM using mirror reflection and rotation to control laser beam movement, EBM relies on magnetic field generated by magnetic deflection coil to control electron beam to move faster without any inertia, and thereby has a faster processing rate [77–79]. Moreover, EBM process is carried out in a vacuum environment, and has the advantages including high energy utilization, no reflection, and high power density, especially suitable for the preparation of RHEAs and brittle materials.

The researches of preparing RHEA by AM method are still in the exploratory stage at present, and focus on laser direct energy deposition technology. For RHEAs, the researches on AM technology still face many challenges. For example, high melting point characteristics of RHEA

greatly increase the difficulties of the preparation of AM metal powders, and many basic forming problems such as light powder action in the AM process have not been made clear. Due to high distortion stress and the internal stress caused by rapid cooling during the AM process, how to suppress the crack during the AM process and how to use the process characteristics of AM technology to achieve good performance of RHEAs, are research directions worth exploring in the future.

2.3 Plastic Deformation and Related Mechanism

The reported structures of RHEAs are mostly confirmed as BCC structures and/or second phases, leading to poor deformability, especially at room temperature [24, 42, 80]. Plastic deformation is an important route to promote deformability and optimize microstructures and performance. Although less work on plastic deformation behavior has been conducted for BCC RHEAs compared with face-centered cubic (FCC) HEAs in the current literatures, more attention to the improvement of RHEAs' deformability has been attracted since 2015 [81–83].

2.3.1 Hot Compression Deformation Under Uniaxial Loading

Various deformation modes studied on RHEAs' plastic deformation can be divided into compression deformation under uniaxial loading [84], and complex deformation under multi-axial loading including rolling [85], hot forging [86] and severe plastic deformation [87]. In particular, compression deformation under uniaxial loading is the most frequently studied, and can better characterize the intrinsic deformation behavior including flow behavior, microstructure evolution and dynamic recrystallization (DRX).

Eleti et al. [84, 88] studied hot deformation behavior at temperatures ranging from 1000 to 1200 °C and with strain rates from 10^{-4} to 10^{-2} s $^{-1}$, and systematically analyzed DRX microstructure evolution and grain boundary

sliding (GBS) of HfNbTaTiZr RHEA at 1000 °C and 10^{-3} s $^{-1}$. Grain boundary (GB) bulging was considered as significant nucleation of DRX grains, as shown in Figure 17. The occurrence of DRX with fine-grained structure was observed under most deformation conditions. The apparent activation energy, high strain rate sensitivity and very limited DRX grain growth were probably related to sluggish diffusion. Heterogeneous DRX microstructures composed of coarse unrecrystallized regions and fine DRX necklace grains were finally formed at larger strains. GBS mechanism was confirmed to dominate deformation in fine-grained DRX regions, while dislocation slip mechanism occurred in the coarse unrecrystallized grains.

Dong et al. [89] revealed hot deformation mechanism and constructed processing map of MoNbHfZrTi RHEA over temperatures ranging from 1100 to 1250 °C and with strain rates varying from 10^{-3} to 0.5 s $^{-1}$. The optimal processing window was determined to be at 1110–1170 °C and 10^{-3} – $10^{-2.5}$ s $^{-1}$, as shown in Figure 18, and only one unstable region as 1100–1220 °C and $10^{-1.5}$ –0.5 s $^{-1}$ with detailed microstructure examination including surface cracks. DRX occurred with fine and undistorted grains at initial GBs, and DRX grains with necklace morphologies gradually formed along grain boundaries and shear bands, and the proportion and size were found to increase with the decrease of strain rate and the increase of temperature.

Liu et al. [90] fabricated ultrafine-grained MoNbTaTiV RHEA by powder metallurgy (P/M) and studied hot deformation behavior at temperature from 1100 to 1300 °C and with strain rate from 0.0005 to 0.5 s $^{-1}$. Work hardening was exhibited in the flow stress curves at 1100 °C, 0.5 s $^{-1}$ and 1200 °C, 0.5 s $^{-1}$. DRX mechanism promoted by ultrafine precipitated phases, as shown in Figure 19, changed from DDRX to CDRX with temperature increasing and strain rate decreasing. Grain growth was limited due to sluggish diffusion and the

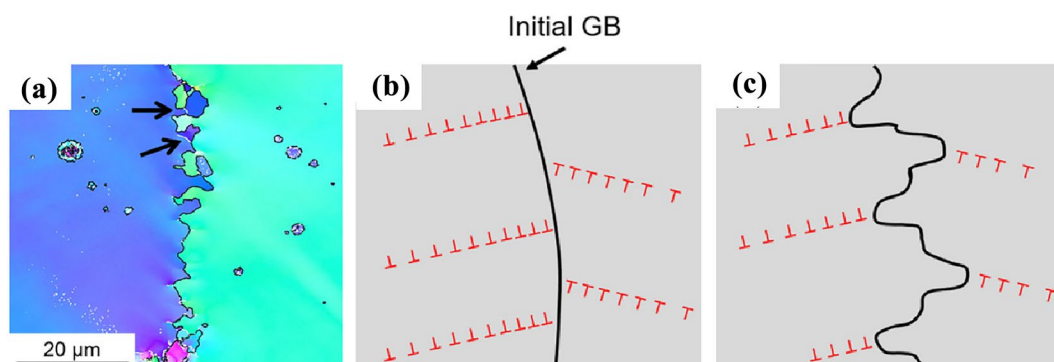


Figure 17 Initial microstructure of DRX grains and schematic illustrations of DRX nucleation mechanism [88] **(a)** the bulging of initial grain boundary, **(b)** dislocations pile-up at an initial grain boundary and **(c)** strain induced boundary migration in the schematic illustrations

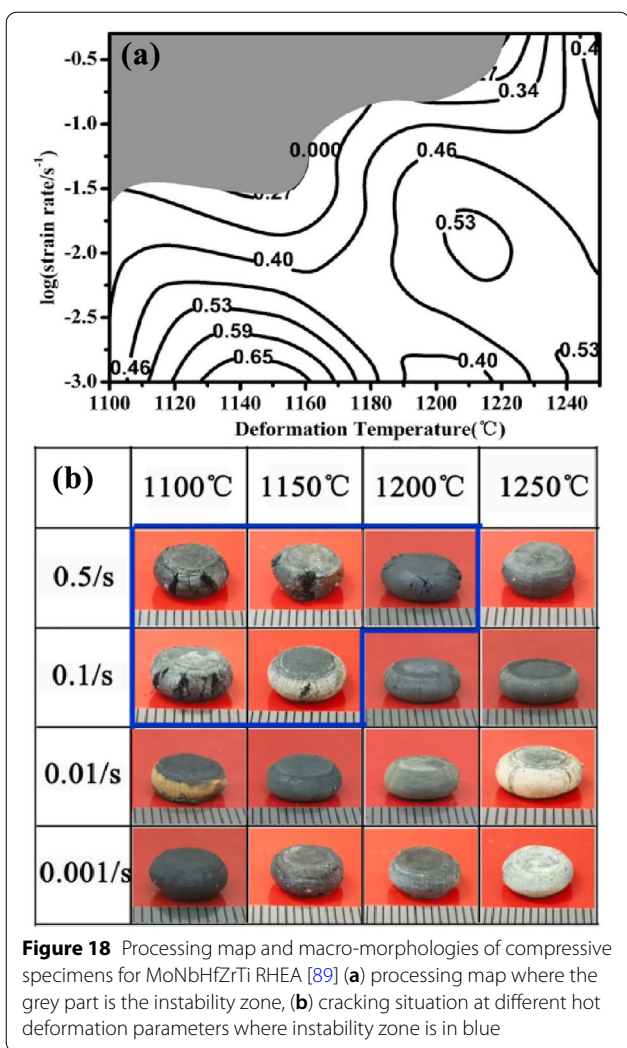


Figure 18 Processing map and macro-morphologies of compressive specimens for MoNbHfZrTi RHEA [89] (a) processing map where the grey part is the instability zone, (b) cracking situation at different hot deformation parameters where instability zone is in blue

pinning of ultrafine precipitated phases. Besides, grain deformation played an important role at low temperature and high strain rate. GBS were confirmed to be the dominant deformation mechanism at higher temperature and lower strain rate.

Cao et al. [91] investigated strain-rate-dependent deformation behavior of $Ti_{29}Zr_{24}Nb_{23}Hf_{24}$ RHEA at temperatures from 700 to 1100 °C and strain rates from 10^{-3} to 10 s⁻¹. Substantial increase in yield stress was observed with the increase of strain rate. High strain rate sensitivity derived was attributed to HEA's high Peierls stress. EBSD examination indicated DRX microstructure evolution with ~50% at different temperatures and strain rates, as shown in Figure 20. The tendency from strain softening to strain hardening in the flow stress was clear with increasing strain rate, indicating a change from dislocation climbing to multiple dislocation slip.

2.3.2 Plastic Deformation Under Complex Loading

As potential high temperature structural materials, studies of BCC RHEAs on other loading conditions, such as cold rolling [85, 92–95] and severe plastic deformation [82], and so on, are also vital to evaluate the applicable hot working and/or further transform as-processed HEAs. Detailed analyses of related deformed microstructures and mechanical properties are beneficial to understand and control the process of hot working.

In the investigation of the process of cold rolling, Senkov et al. [92] observed grain elongation and deformation bands in the cold rolled HfNbTaTiZr RHEA with 65% and 85% thickness reductions. Partial and complete recrystallization occurred after subsequent annealing at 800 and 1000 °C. Eleti et al. [93] demonstrated that the development of deformation microstructure of HfZrTi-TaNb RHEA was accompanied by extensive deformation heterogeneities with strain up to 90%, and deformation heterogeneities significantly influenced the formation of the cold-rolling and annealing textures, as shown in Figure 21. Yurchenko et al. [94] studied microstructure evolution of as-cast $Ti_{1.89}CrNb_{0.56}$ RHEA during cold rolling to a thickness strain of 80%. The formation of dislocation substructure and development of kink and shear bands were observed. Wu et al. [95] elucidated the deformation mechanism of HfNbTaTiZr RHEA alloy subjected to cold rolling. Microstructure evolution during the whole cold rolling was divided into five stages as follows: ① dislocation tangles, ② microbands, ③ thin laths and microshear bands containing thin laths, ④ the transverse breakdown of the lath to elongated segment, and ⑤ fine grains.

Besides, deformation behavior and microstructure evolution were studied in the hot-forged and severe plastic deformed conditions. The decomposition of primary BCC phase into BCC (Ti, Nb, Ta)-rich matrix and HCP (Zr, Al)-rich precipitates occurred after hot forging of $TiNbTa_{0.5}ZrAl_{0.5}$ P/M RHEA [86]. High pressure torsion (HPT) resulted in the refinement of as-cast $AlNbTiVZr_{0.5}$ alloy in the form of nanocrystalline structure attributed to shear banding [87]. Meanwhile, the network of laves phase was broken and individual particles became much thinner in the HPTed condition compared with in the as-cast condition.

2.4 Microstructure Control by Heat Treatment

Heat treatment is a significant process to improve deformability and mechanical properties and to eliminate residual stress of RHEAs. And microstructures, especially second phases, can be tailored by heat treatment parameters including temperature, holding time and cooling rate, finally affecting mechanical properties

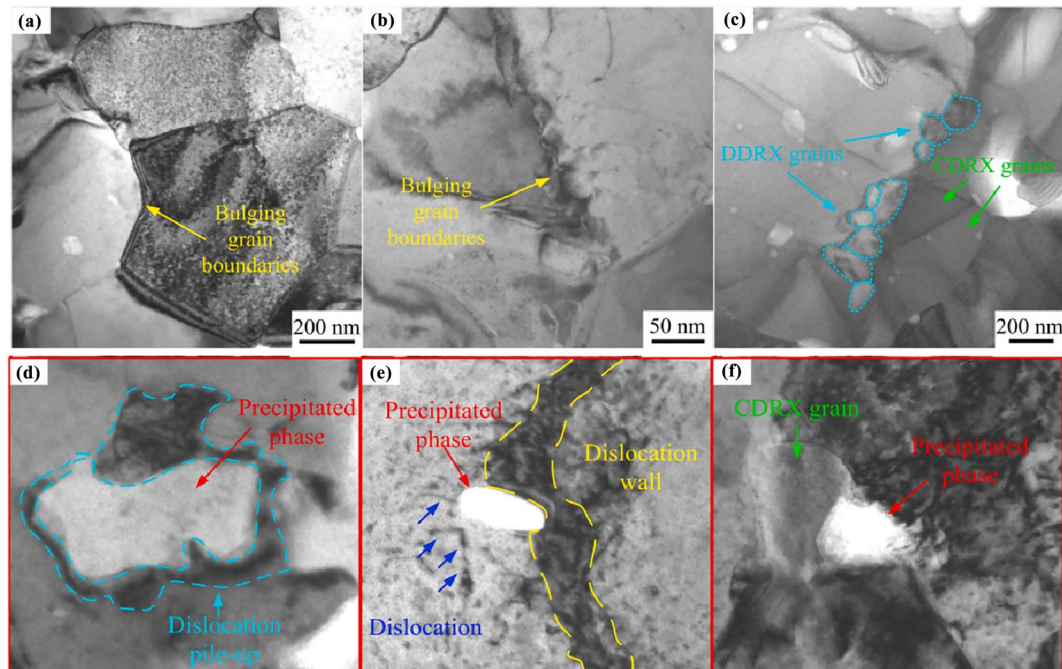


Figure 19 TEM images of deformed MoNbTaTiV RHEA [90] (a) and (b) bulging GBs, (c) DDRXed grains and CDRXed grains, (d) precipitates at GBs, (e) precipitates in the grain, (f) precipitates at the trigeminal GBs

of RHEAs. Therefore, it is instructive to study the effects of heat treatment on microstructure for the selection of the reasonable heat treatment parameters.

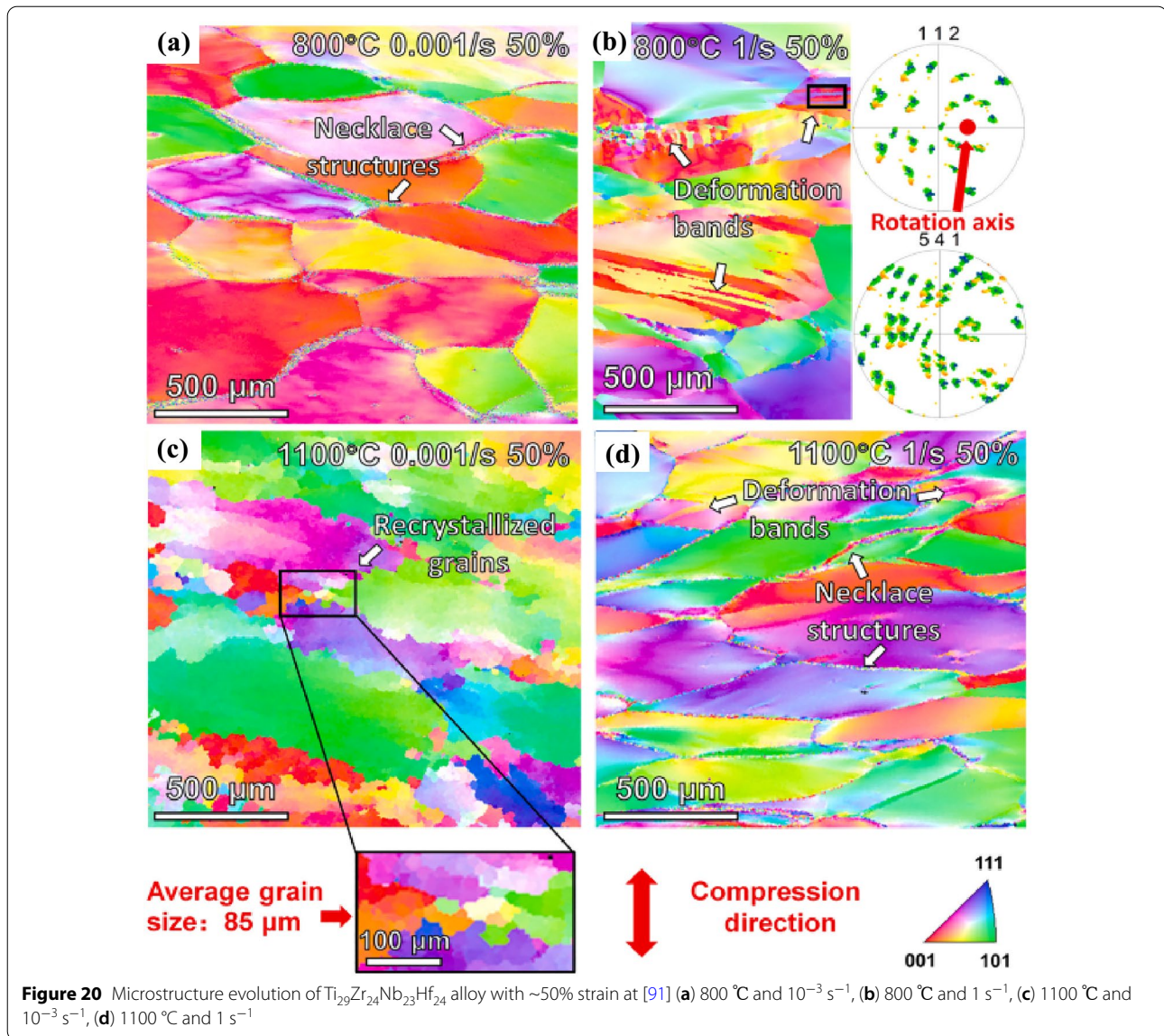
2.4.1 Microstructure Evolution by Heat Treatment Prior to Deformation

Heat treatment prior to deformation, for example, homogenization heat treatment, is considered as an important way to improve deformability via microstructure control. Generally, micro-segregation would be present in the as-cast RHEAs due to different melting points of elements [96], resulting in poor deformability and inhomogeneous microstructure. Consequently, homogenization treatment at high temperature and long holding time with a certain cooling rate should be utilized to eliminate element segregation and to tailor the as-cast microstructure, especially phase structure.

Lee et al. [97] found that chemical segregation and microstructural inhomogeneity were completely eliminated by homogenization treatment at 1200 °C for 3 days. Yurchenko et al. [98] observed that single B2 structure remained in the as-homogenized condition at 1200 °C for 24 h as that in the as-cast condition for $\text{Ti}_{40}\text{Nb}_{30}\text{Hf}_{15}\text{Al}_{15}$. Stepanov et al. [99] found that BCC solid solution remained in the as-homogenized NbTiVZr alloy, while C14 laves and Zr_2Al phases was precipitated in BCC matrix for $\text{Al}_x\text{NbTiVZr}$ ($x = 0.5, 1, 1.5$).

Yang et al. [45] investigated microstructure evolution after different homogenized treatments at 1000 °C for 24 h, 1200 °C for 24 h, 1400 °C for 24 h, and 1450 °C for 168 h, as shown in Figure 22. hcp-1 phase was precipitated at 1000 °C and gradually dissolved up to 1200 °C. The disappearance of hcp-1 phase and the formation of fine nanoprecipitates occurred at 1400 °C. After annealing at 1450 °C for one week, the BCC phase decomposition into two kinds of new FCC phases occurred with fine nanoprecipitate only remaining in BCC matrix and another new hcp-2 phase forming in the grain.

Soni et al. [100] observed subtle change from a two-phase B2+BCC mixture to a nano-scale mixture of co-continuous BCC and B2 phases, resembling a spinodally decomposed microstructure with concurrent ordering after homogenization treatment at a high-temperature, followed by fast or slow cooling to room temperature for the $\text{Al}_{0.25}\text{NbTaTiZr}$ RHEA. Yurchenko et al. [101] found that composite-like hypoeutectic microstructure comprised of softer primary B2 phase and harder eutectic mixture consisting of C14 Laves and B2 phases was retained, and a small amount of Zr_5Al_3 -type phase formed after homogenizing at 1200 °C, as shown in Figure 23.



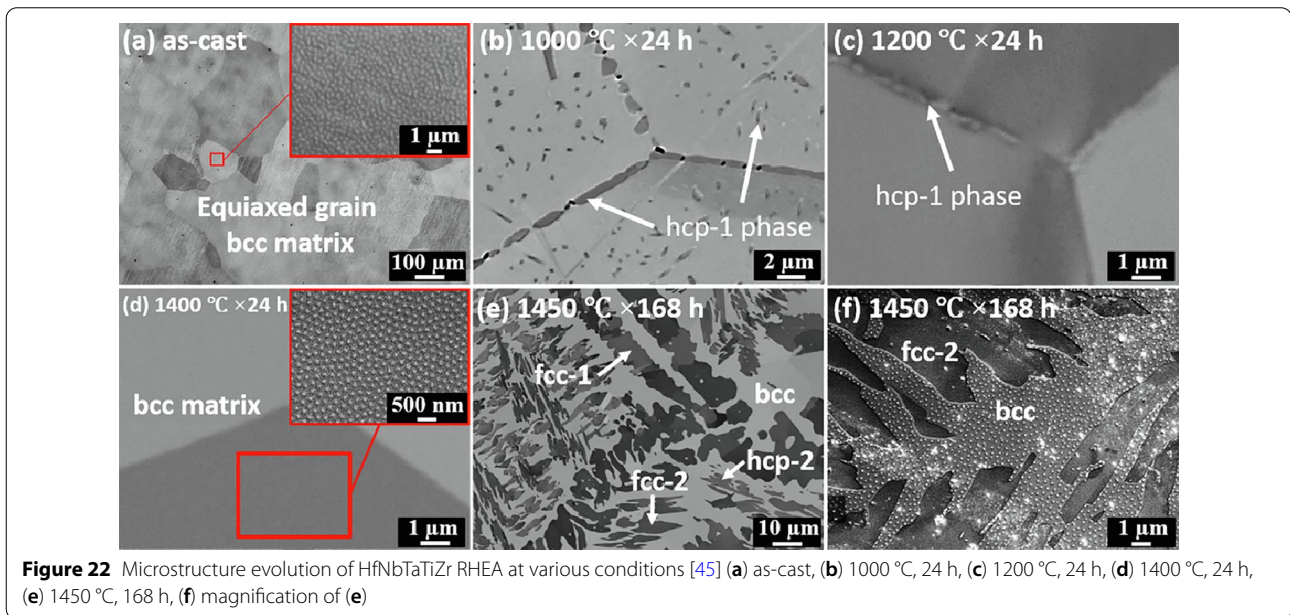
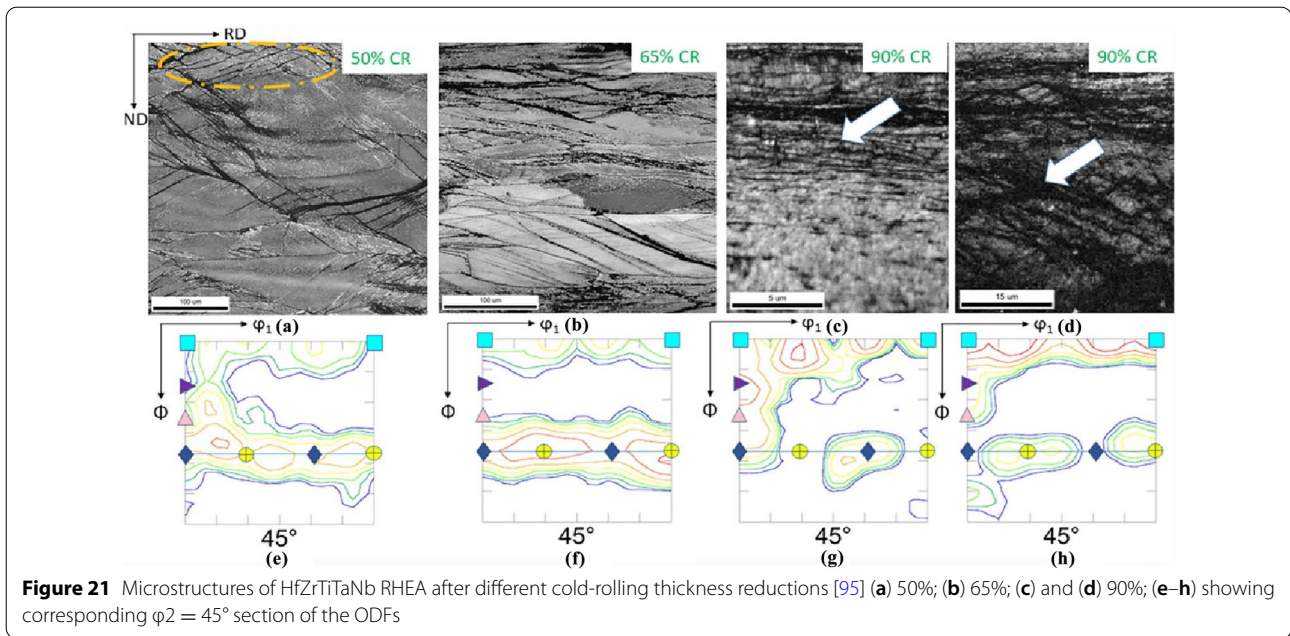
2.4.2 Microstructure Evolution After Annealing Heat Treatment and Aging Heat Treatment

Heat treatments such as annealing treatment [85] and aging treatment [28], are regarded as significant processes controlling grain structure and the precipitation behavior and improving the resultant mechanical properties. Therefore, the effects of annealing heat treatment and aging heat treatment on microstructure evolution of a series of RHEAs were elaborated in the following description.

In the reported literatures on aging heat treatment, Wang et al. [102] found that the coarsening of cuboidal nanoprecipitates with a size of 25–50 nm occurred in the $\text{Al}_{0.4}\text{Nb}_{0.5}\text{Ta}_{0.5}\text{TiZr}_{0.8}$ RHEA due to a moderate lattice misfit after aging 873 K, and Zr_5Al_3 phase also coexisted

with B2. But the deterioration of the BCC/B2 coherency occurred with aging temperature, leaving coarse Zr_5Al_3 phase alone. The formation of Widmanstatten (Ti, Al)-rich orthorhombic particles (O-phase) in BCC matrix were detected in the $\text{Ti}_{40}\text{Nb}_{30}\text{Hf}_{15}\text{Al}_{15}$ RHEA after aging heat treatment at 600°C for 24 h [98]. The formation of additional ordered omega type AlZr_2 phase in $\text{Al}_{10}\text{Nb}_{15}\text{Ta}_5\text{Ti}_{30}\text{Zr}_{40}$ RHEA when aging at 600°C and 750°C [100].

Soni et al. [103] investigated microstructure evolution of $\text{Al}_{0.5}\text{NbTa}_{0.8}\text{Ti}_{1.5}\text{V}_{0.2}\text{Zr}$ RHEA during aging at 600°C . Spinodal decomposition into a continuous B2 matrix with discrete cuboidal BCC precipitates aligned along the $\langle 001 \rangle$ directions was changed from a co-continuous mixture of a disordered BCC and an ordered B2 phase



into when aging at 600 °C. And the development of necking constrictions along the B2 channels, eventually pinching-off these channels and making the BCC phase continuous with discrete B2 precipitates were observed with different aging times at 600 °C, as shown in Figure 24. Yurchenko et al. [104] studied the aging behavior of $AlCr_xNbTiV$ and $AlNbTiVZr_x$ ($x = 0-1.5$) RHEAs at 800 or 1000 °C. The precipitation of Nb_2Al -type s-phase or an increase in the fraction of Laves phase in the aged $AlCr_xNbTiV$ ($x = 0-1.5$) alloy, caused an increase in

the microhardness and a pronounced drop in ductility. Annealing of the $AlNbTiVZr_x$ ($x = 0.5-1.5$) alloys at 800 or 1000 °C led to insignificant changes in the structure and microhardness but somewhat decreased ductility.

Concerning the annealing after cold rolling, Yurchenko et al. [94] pointed out that the precipitation of Cr-rich FCC (C15) laves phase occurred after annealing at 800 °C for the as-rolled $Ti_{1.89}CrNbV_{0.56}$ RHEA. A fine duplex microstructure was obtained via recrystallization along with laves phase after annealing at 1000 °C. A coarse-grained

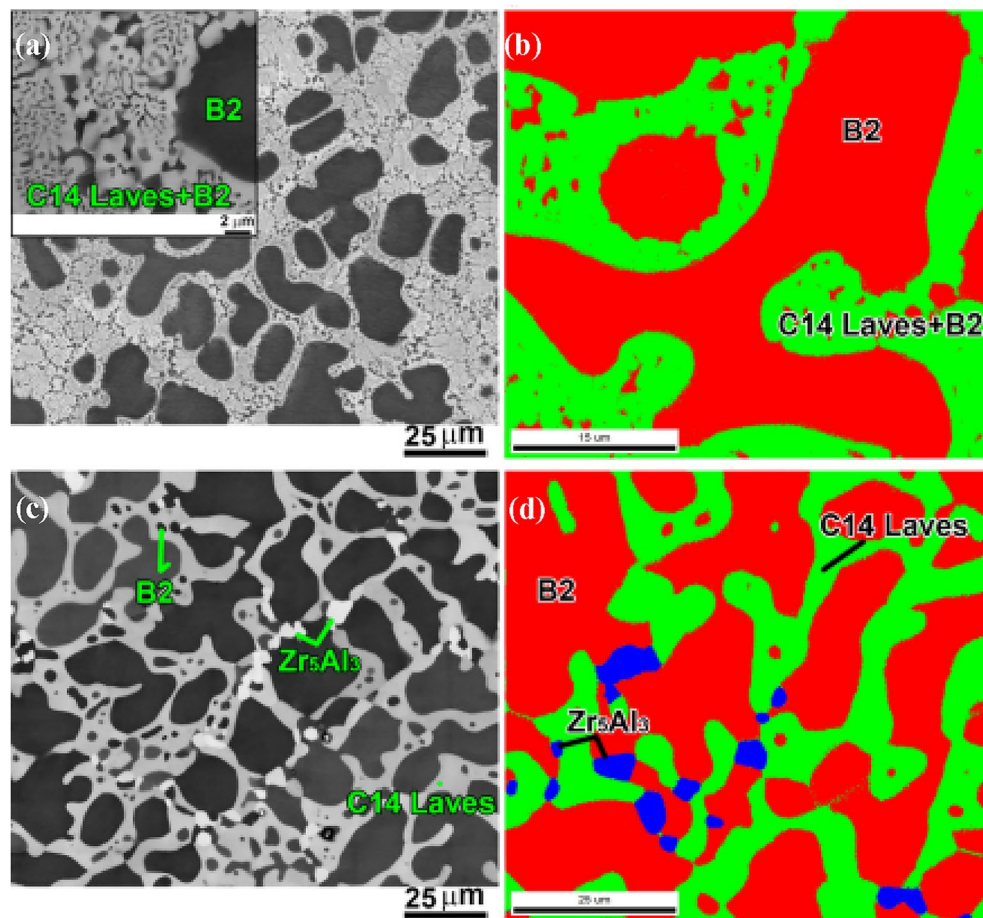


Figure 23 Microstructures evolution of Al₂₀Cr₁₀Nb₁₅Ti₂₀V₂₅Zr₁₀ alloy [101] (a) SEM image and (b) phase map in the as-cast condition; (c) SEM image and (d) phase map in the as-homogenized condition

recrystallized single-phase BCC microstructure was observed with annealing temperature increasing to 1200 °C. Tu et al. [105] elucidated microstructure evolution and hardening effect of 80% cold-rolled HfNbTiZr specimens after annealing at 450 °C. The precipitation of needle-like HCP phase with a composition of HfTiZr near the GB and particle-like Ni-rich BCC phase within the grain occurred after annealing for more than 10 h. 49% increase of hardness was detected after annealing for 100 h due to HCP and BCC precipitates. However, the presence of HCP and BCC precipitates was considered to induce brittleness due to a dramatic change in the hardness for the annealed specimens with a shorter aging time, indicating that cold rolling can dramatically lower the initiation point of hardening.

3 Outlook

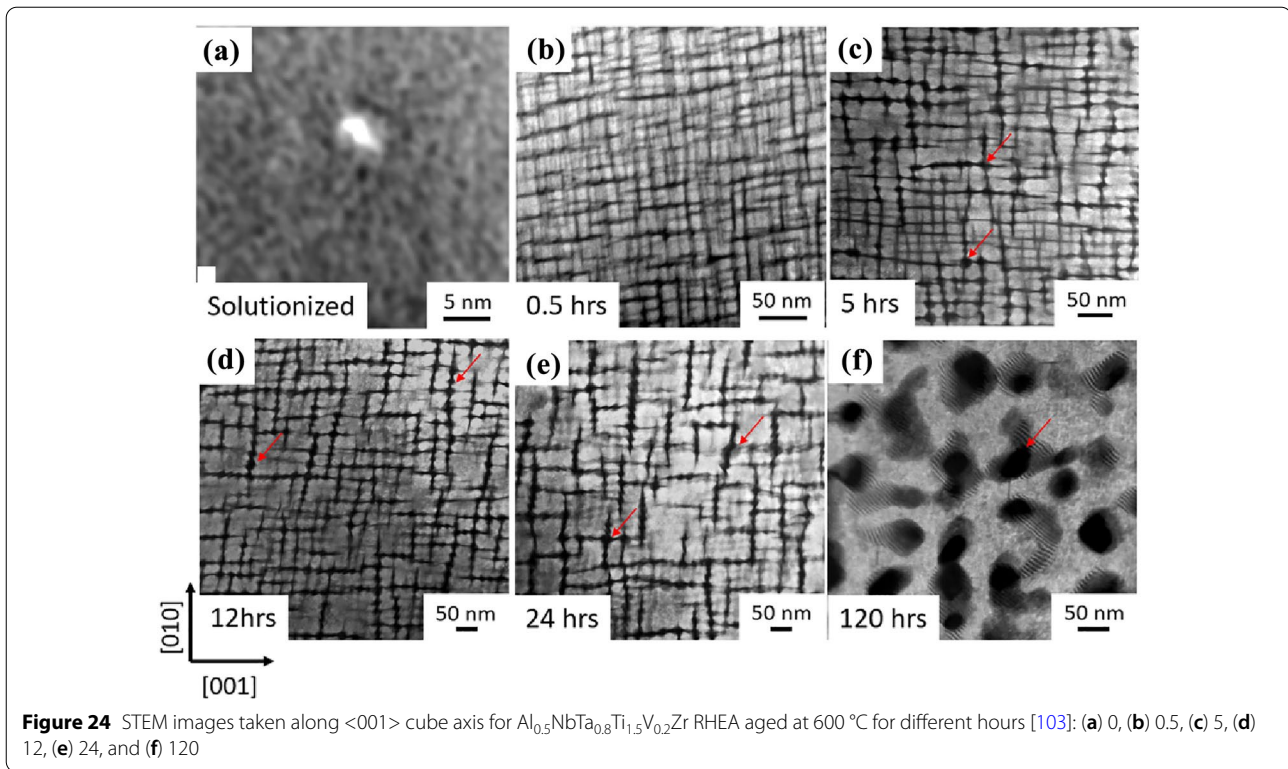
3.1 High-throughput Screening Preparation and Tests for RHEAs with Excellent Performance

In the past decade, great progress has been made in the research of RHEAs, and more than 100 alloy systems

have been developed. However, it is still difficult to find the alloy composition with optimum performance in a short research term. The RHEAs may have more than 30000 alloy combinations, and there are still many unknown systems that need to be explored.

The complex structure of RHEAs brought many problems in the design of RHEAs. For example, the formation of the brittle C14 Laves phase in the BCC-base RHEAs would significantly deteriorate the properties because the dissimilarity of crystal structures and different thermal expansion coefficients would increase cracking tendency of the RHEAs [106]. Hence, exploring suitable chemical compositions without the formation of detrimental intermetallic phases is crucial for developing the desirable materials.

However, the vastness of the compositional space poses a huge challenge for efficiently screening out those suitable compositions. For this, obviously, the traditional trial-and-error experimental method is no longer suitable, since it is extremely costly and time-consuming



to experimentally screen the proper alloys [107]. Fortunately, the pace of discovering promising RHEAs could be accelerated by the development of efficient computational screening methods and tools [108, 109]. Most of the calculation methods use the CALculation of PHAseDiagrams (CALPHAD) or first-principle method. CALPHAD can be used to predict single-phase solid solution alloys and their components [110–112]. The first-principle calculation can be used to calculate the phase stability, lattice parameters, electronic structure, elastic coefficient, diffusion coefficient as well as thermodynamic properties of RHEAs with BCC structure [113, 114].

At present, there is still a lack of necessary high-throughput experiments, and the structural characterization and model of refractory high entropy alloys are not clear. Therefore, it is urgently needed to develop high-throughput experiments and calculation methods to efficiently explore the wide range of refractory high entropy alloy systems and structural models.

3.2 Advanced Feasible Hot Working

The plastic deformation behavior of BCC RHEAs was summarized in this work. The current researches on deformation behavior of RHEAs are mainly based on conventional deformation models, such as constitutive relation and processing map, and the studies available

on deformation mechanisms have shown similar characteristics including dislocation patterning, slip plane, dislocation climbing, etc, to those of conventional materials. However, long-range disorder, lattice distortion and sluggish diffusion are featured in the HEAs, causing that Burgers vector of dislocation may no longer be a constant value. It is necessary to modify the conventional deformation with introducing RHEA's characteristics and establish predictive deformation model and mechanism suitable for RHEAs.

The effects of different hot deformation parameters including deformation temperature, strain rate and strain on ultimate mechanical properties of RHEAs are still on questions, although more deformation behavior of RHEAs was characterized. It is hard to illustrate the validation of the selection of deformation parameters. Therefore, more attention should be paid to the selection of deformation parameters and their effects on mechanical properties of RHEAs for clarifying advanced feasible hot working.

3.3 Microstructure Control by Heat Treatment for Improving Deformability and Performance

The effects of pre-deformation homogenization heat treatment and post-deformation heat treatment including aging and annealing on precipitates, phase structure and microstructure of RHEAs were summarized.

However, no unified conclusion on the mechanism of heat treatment on RHEAs is made due to no systematical and comprehensive researches. Therefore, it is crucial to clarify the transformation mechanism of RHEAs during heat treatment in the future work.

The effect of heat treatment on RHEAs is also closely related to element types and heat-treatment methods. In order to clarify the effects of heat treatment on improving deformability and/or mechanical property, for the researches on the effects of element types and heat-treatment methods on heat treatment, more attention should be paid to the following points: ① For the effects of element types, the clarification of the mechanism of different elements during heat treatment should be made due to the large differences in heat treat behaviors for RHEAs with different element types. ② For the effects of heat-treatment methods, new definition of different heat-treatment methods and their related mechanisms for RHEAs should be clarified, because no phase diagram is used as a guide in the current RHEA, which is of great significance to the research on heat treatment of RHEAs in the future and to the actual production.

3.4 Investigation of Comprehensive Properties

The mechanical properties of RHEAs are related to alloy composition, phase constituents, principal component content and preparation process. At room temperature, most of RHEAs possess high-strength and low toughness. Meanwhile, RHEAs exhibit high-strength and high toughness at high temperature, showing their potential used as high-temperature structures. Due to the different atomic sizes for those elements, the atoms in HEAs tend to deviate from their ideal lattice sites and give rise to severe local lattice distortion [71, 115], which could impede dislocation motion, leading to the pronounced strengthening effects [116, 117].

In addition, because the RHEAs are composed of five or more refractory metals in equal atomic ratio or near equal atomic ratio, the main elements diffuse with each other during diffusion and the new phase will hardly grow up. Therefore, nano-phases are often precipitated, which can also improve the strength and hardness of RHEAs. The element constituents are the key factors for the alloy to show high strength and hardness.

Most of the alloying elements in RHEAs are rare and expensive, so they have no obvious advantages over traditional metals and alloys in the cost aspect. The future application for RHEAs should be focused on special materials serving under extreme conditions, especially in extreme environments such as some important equipment, aerospace and nuclear reactors with harsh requirements for hot components.

Considering the working environment of the refractory high entropy alloy, besides the mechanical properties, the studies of mechanics, oxidation resistance, corrosion resistance and other properties in extreme environments should be concerned in the future. For example, the high-temperature oxidation resistance is also very important. In order to improve the high-temperature oxidation resistance of the refractory high entropy alloy, the anti-oxidation elements such as Al, Cr, Ti and Si are usually added [118].

Zhang et al. [119] studied the oxidation behavior of NbCrMoAl_{0.5} (Ti or V or Si = 0.3) series alloys, and the results showed that the addition of Ti and Si increased the oxidation resistance, while the reduction of oxidation resistance occurred with V addition. Zhang et al. [120] studied oxidation response of the NbZrTiCrAl refractory high entropy alloy at 800, 1000 and 1200 °C, respectively. The result showed that the oxidation of the alloy at 800 and 1000 °C followed parabolic rate law, and the protection performance can be attributed to the formation of dense and homogenous complex oxides scale composed of CrNbO₄, ZrO₂, TiO₂, Al₂O₃ and ZrNb₂O₇. For the traditional refractory alloy, the poor oxidation resistance is regarded as a serious potential barrier to the long-term application of the RHEAs at elevated temperatures [121].

Previous studies have shown that RHEAs exhibited excellent properties in extreme environments such as extremely high temperature, oxidation, wear, corrosion and irradiation, but there are few studies on service behavior and failure mechanism in multi field coupling environment, which will be one of the future research directions of RHEAs. Additionally, RHEAs have shown better high temperature strength than traditional nickel base superalloys, but the brittleness problem at room temperature still needs to be solved.

In summary, how to realize the combination of high strength at high temperature and good ductility at room temperature, and how to improve the toughness at room temperature and high-temperature oxidation resistance and to decrease the density of the RHEAs, have become the important research issues in this field [115, 119, 121–123].

Acknowledgements

Not applicable.

Author contributions

QY, HX and XX conceived the idea of the study; XX wrote the manuscript; NL, WL, SH, QY, EW and XH provided the data. All authors read and approved the final manuscript.

Authors' Information

Xiaochang Xie, born in 1984, is currently a PhD student at *University of Science and Technology Beijing, China*, and also a senior engineer at *Beijing Institute of Aeronautical Materials, China*. He received his master degree in materials processing engineering from *University of Science and Technology Beijing, China*, in 2009.

Neng Li, born in 1985, is currently a senior engineer at *Beijing Institute of Aeronautical Materials, China*. He received his PhD degree in materials science and engineering from *Beijing Institute of Aeronautical Materials, China*, in 2019.

Wei Liu, born in 1984, is currently a senior engineer at *Beijing Institute of Aeronautical Materials, China*. He received his PhD degree in materials science and engineering from *Beihang University, China*, in 2015.

Shuai Huang, born in 1989, is currently a senior engineer at *Beijing Institute of Aeronautical Materials, China*. He received his PhD degree in condensed matter physics from *Beihang University, China*, in 2017.

Xiaoyong He, born in 1994, is currently an engineer at *Beijing Institute of Aeronautical Materials, China*. He received his master degree in solid mechanics from *Tianjin University, China*, in 2020.

Qiuying Yu, born in 1984, is currently a senior engineer at *Beijing Institute of Aeronautical Materials, China*. She received her PhD degree in materials science and engineering from *University of Science and Technology Beijing, China*, in 2014.

Huaping Xiong, born in 1969, is currently a professor and a PhD candidate supervisor at *Beijing Institute of Aeronautical Materials, China*. His main research interests include welding and joining, and additive manufacturing.

Enhui Wang, born in 1990, is currently an associate professor at *University of Science and Technology Beijing, China*. He received his PhD degree in metallurgical engineering from *University of Science and Technology Beijing, China*, in 2019.

Xinmei Hou, born in 1979, is currently a professor at *University of Science and Technology Beijing, China*. She received her PhD degree in metallurgical engineering from *University of Science and Technology Beijing, China*, in 2009.

Funding

Supported by National Natural Science Foundation of China (Grant Nos. U2141205, 51775525, 52175369, 52005465, 52025041 and 52174294), Fast Support Program (Grant No. 80923020405), Beijing Nova Program from Beijing Municipal Science & Technology Commission (Grant No. Z201100006820094).

Availability of Data and Materials

All data generated or analysed during this study are included in this published article. All data are fully available without restriction.

Competing Interests

The authors declare no competing financial interests.

Author Details

¹Collaborative Innovation Center of Steel Technology, University of Science and Technology Beijing, Beijing 100083, China. ²Beijing Institute of Aeronautical Materials, Beijing 100095, China.

Received: 28 June 2022 Revised: 26 October 2022 Accepted: 28 October 2022

Published online: 30 November 2022

References

- [1] M M Bakradzeya, S V Ovsepyana, A A Buiakina, et al. Development of Ni-base superalloy with operating temperature up to 800 °C for gas turbine disks. *Inorganic Materials: Applied Research*, 2018, 9(6): 1044-1050.
- [2] T M Pollock. Alloy design for aircraft engines. *Nature Materials*, 2016, 15(8): 809-815.
- [3] H Jiang, J X Dong, M C Zhang, et al. Development of typical hard-to-deform nickel-base superalloy for turbine disk served above 800 °C. *Aeronautical Manufacturing Technology*, 2021, 64(1/2): 62-73. (in Chinese)
- [4] R G Crookes, B März, H Z Wu. Ductile deformation in alumina ceramics under quasi-static to dynamic contact impact. *Materials and Design*, 2020, 187: 108360.
- [5] A Lasalmonie. Intermetallics: why is it so difficult to introduce them in gas turbine engines? *Intermetallics*, 2006, 14: 1123-1129.
- [6] B Gorr, H J Christ, D Mukherji, et al. Thermodynamic calculations in the development of high-temperature Co-Re-based alloys. *Journal of Alloys and Compounds*, 2014, 582: 50-58.
- [7] J W Yeh, S K Chen, S J Lin, et al. Nanostructured high-entropy alloys with multiple principal elements: novel alloy design concepts and outcomes. *Advanced Engineering Materials*, 2004, 6(5): 299-303.
- [8] B Cantor, I T H Chang, P Knight, et al. Microstructural development in equiatomic multicomponent alloys. *Materials Science and Engineering A*, 2004, 375-377: 213-218.
- [9] J W Yeh. Alloy design strategies and future trends in high-entropy alloys. *JOM*, 2013, 65(12): 1759-1771.
- [10] Y J Zhou, Y Zhang, F J Wang, et al. Phase transformation induced by lattice distortion in multiprincipal component CoCrFeNiCu_xAl_{1-x} solid-solution alloys. *Applied Physics Letters*, 2008, 92: 241917.
- [11] K Y Tsai, M H Tsai, J W Yeh. Sluggish diffusion in Co-Cr-FeMn-Ni high-entropy alloys. *Acta Materialia*, 2013, 61: 4887-4897.
- [12] Z P Lu, H Wang, M W Chen, et al. An assessment on the future development of high-entropy alloys: summary from a recent work-shop. *Intermetallics*, 2015, 66: 67-76.
- [13] T K Tsao, A C Yeh, C M Kuo, et al. The high temperature tensile and creep behavior of high entropy superalloy. *Scientific Reports*, 2017, 7(1): 12658.
- [14] S Y Wang, S J Song, X C Lu, et al. Tensile fracture behavior of the CrMn-FeCoNi high entropy alloy: a crystal plasticity finite element simulation. *Journal of Mechanical Engineering*, 2021, 57(22): 43-51. (in Chinese)
- [15] M X Ma, Z X Wang, J C Zhou, et al. Effect of Ti doping on microstructure and wear resistance of CoCrCuFeMn high-entropy alloys. *Journal of Mechanical Engineering*, 2020, 56(10): 110-116. (in Chinese)
- [16] O N Senkov, G B Wilks, D B Miracle, et al. Refractory high-entropy alloys. *Intermetallics*, 2010, 18(9): 1758-1765.
- [17] J Chen, X Y Zhou, W L Wang, et al. A review on fundamental of high entropy alloys with promising high-temperature properties. *Journal of Alloys and Compounds*, 2018, 760: 15-30.
- [18] O N Senkov, D Isheim, D N Seidman, et al. Development of a refractory high entropy superalloy. *Entropy*, 2016, 18: 102-114.
- [19] O N Senkov, G B Wilks, J M Scott, et al. Mechanical properties of Nb₂₅Mo₂₅Ta₂₅W₂₅ and V₂₀Nb₂₀Mo₂₀Ta₂₀W₂₀ refractory high entropy alloys. *Intermetallics*, 2011, 19: 698-706.
- [20] O N Senkov, D B Miracle, K J Chaput, et al. Development and exploration of refractory high entropy alloys-A review. *Journal of Materials Research*, 2018, 33: 3092-3128.
- [21] J P Couzinié, O N Senkov, D B Miracle, et al. Comprehensive data compilation on the mechanical properties of refractory high-entropy alloys. *Data in Brief*, 2018, 21: 1622-1641.
- [22] O N Senkov, S Gorse, D B Miracle. High temperature strength of refractory complex concentrated alloys. *Acta Materialia*, 2019, 175: 394-405.
- [23] O N Senkov, C Woodward, D B Miracle. Microstructure and properties of aluminum-containing refractory high-entropy alloys. *JOM*, 2014, 66: 2030-2042.
- [24] O N Senkov, C F Woodward. Microstructure and properties of a refractory NbCrMo_{0.5}Ta_{0.5}TiZr alloy. *Materials Science and Engineering A*, 2011, 529: 311-320.
- [25] C C Juan, M H Tsai, C W Tsai, et al. Enhanced mechanical properties of HfMoTaTiZr and HfMoNbTaTiZr refractory high-entropy alloys. *Intermetallics*, 2015, 62: 76-83.
- [26] Z Guo, A Zhang, J Han, et al. Effect of Si additions on microstructure and mechanical properties of refractory NbTaWMo high-entropy alloys. *Journal of Materials Science*, 2019, 54: 5844-5851.
- [27] S Y Chen, Y Tong, K K Tseng, et al. Phase transformations of HfNbTaTiZr high-entropy alloy at intermediate. *Scripta Materialia*, 2019, 158: 50-56.
- [28] N D Stepanov, N Y Yurchenko, S V Zhrebtsov, et al. Aging behavior of the HfNbTaTiZr high entropy alloy. *Materials Letter*, 2018, 211: 87-90.
- [29] B S Murty, J W Yeh, S Raganathan. *High-entropy Alloys*. London: Butterworth-Heinemann, 2014.
- [30] M Wang, Z Ma, Z Xu, et al. Designing VNbMoTa refractory high-entropy alloys with improved properties for high-temperature applications. *Scripta Materialia*, 2021, 191: 131-136.
- [31] Z D Han, N Chen, S F Zhao, et al. Effect of Ti additions on mechanical properties of NbMoTaW and VNbMoTaW refractory high entropy alloys. *Intermetallics*, 2017, 84: 153-157.
- [32] D B Miracle, O N Senkov. A critical review of high entropy alloys and related concepts. *Acta Materialia*, 2017, 122: 448-511.
- [33] S Ge, H Fu, L Zhang, et al. Effects of Al addition on the microstructures and properties of MoNbTaTiV refractory high entropy alloy. *Materials Science and Engineering A*, 2020, 784: 139275.

- [34] Y Tong, L Bai, X Liang, et al. Influence of alloying elements on mechanical and electronic properties of NbMoTaWx ($x = \text{Cr, Zr, V, Hf}$ and Re) refractory high entropy alloys. *Intermetallics*, 2020, 126: 106928.
- [35] B Liu, J Wang, J Chen, et al. Ultra-high strength TiC/refractory high-entropy-alloy composite prepared by powder metallurgy. *JOM*, 2017, 69: 651-656.
- [36] T J Harrington, J Gild, P Sarker, et al. Phase stability and mechanical properties of novel high entropy transition metal carbides. *Acta Materialia*, 2019, 166: 271-280.
- [37] Y Long, X Liang, K Su, et al. A fine-grained NbMoTaWVCr refractory high-entropy alloy with ultra-high strength: Microstructural evolution and mechanical properties. *Journal of Alloys and Compounds*, 2019, 780: 607-617.
- [38] S Lv, Y Zu, G Chen, et al. A multiple nonmetallic atoms co-doped CrMoNbWTi refractory high-entropy alloy with ultra-high strength and hardness. *Materials Science and Engineering A*, 2020, 795: 140035.
- [39] S Lv, Y Zu, G Chen, et al. An ultra-high strength CrMoNbWTi-C high entropy alloy co-strengthened by dispersed refractory IM and UHTC phases. *Journal of Alloys and Compounds*, 2019, 788: 1256-1264.
- [40] B Kang, T Kong, A Raza, et al. Fabrication, microstructure and mechanical property of a novel Nb-rich refractory high-entropy alloy strengthened by in-situ formation of dispersoids. *International Journal of Refractory Metals and Hard Materials*, 2019, 81: 15-20.
- [41] G Chen, T Luo, S Shen. Research progress in refractory high-entropy alloys. *Materials Review*, 2021, 35(17): 17064-17080.
- [42] O N Senkov, D B Miracle, K J Chaput, et al. Development and exploration of refractory high entropy alloys-A review. *Journal of Materials Research*, 2018, 33(19): 3092-3128.
- [43] G Li, P Cui, L J Zhang. Current studies of high entropy alloys. *Journal of Yanshan University*, 2018, 42(2): 4-13.
- [44] J P Couzinié, G Dirras, L Perrière, et al. Microstructure of a near-equiatomic refractory high-entropy alloy. *Materials Letters*, 2014, 126: 285-287.
- [45] C Yang, K Aoyagi, H Bian. Microstructure evolution and mechanical property of a precipitation-strengthened refractory high-entropy alloy HfNbTaTiZr. *Materials Letters*, 2019, 254: 46-49.
- [46] D Qiao, H Jiang, W Jiao. A novel series of refractory high-entropy alloys $\text{Ti}_2\text{ZrHf}_{0.5}\text{VNbx}$ with high specific yield strength and good ductility. *Acta Metallurgica Sinica (English Letters)*, 2019, 32(8): 925-931.
- [47] Q Y Yu, X Y He, X C Xie, et al. Effects of the variation of alloy composition on microstructures of as-cast AlMoNbTaTiZr high-entropy alloys. *Journal of Mechanical Engineering*, 2021, 57(6): 96-105. (in Chinese)
- [48] M Wang, Z Ma, Z Xu, et al. Microstructure and mechanical properties of HfNbTaTiZrW and HfNbTaTiZrMoW refractory high-entropy alloy. *Journal of Alloys and Compounds*, 2019, 803: 778-785.
- [49] J Y Yu, R D Mu, S Y Qu, et al. The effect of heat treatment at 1200 °C on microstructure and mechanical properties evolution of AlCoCrFeNiSi-YHf high entropy alloys. *Vacuum*, 2022, 200: 111039.
- [50] Y Qiao, Y Tang, S Li, et al. Preparation of TiZrNbTa refractory high-entropy alloy powder by mechanical alloying with liquid process control agents. *Intermetallics*, 2020, 126: 106900.
- [51] J Han, B Su, J Lu, et al. Preparation of MoNbTaW refractory high entropy alloy powders by pressureless spark plasma sintering: Crystal structure and phase evolution. *Intermetallics*, 2020, 123: 106832.
- [52] Y Li, Y Shi. Microstructure and corrosion resistance of laser-deposited AlCrFeCoNiCu coating on aluminum alloy surface. *Chinese Optics*, 2019, 12(2): 344-354.
- [53] O A Waseem, H J Ryu. Powder metallurgy processing of a WxTaTiVCr high-entropy alloy and its derivative alloys for fusion material applications. *Scientific Reports*, 2017, 7(1): 1-14.
- [54] W Guo, B Liu, Y Liu, et al. Microstructures and mechanical properties of ductile NbTaTiV refractory high entropy alloy prepared by powder metallurgy. *Journal of Alloys and Compounds*, 2019, 776: 428-436.
- [55] B Kang, T Kong, H J Ryu, et al. Superior mechanical properties and strengthening mechanisms of lightweight $\text{Al}_x\text{CrNbVMo}$ refractory high-entropy alloys ($x = 0, 0.5, 1.0$) fabricated by the powder metallurgy process. *Journal of Materials Science & Technology*, 2021, 69: 32-41.
- [56] C Zhu, Z Li, C Hong, et al. Microstructure and mechanical properties of the TiZrNbMoTa refractory high-entropy alloy produced by mechanical alloying and spark plasma sintering. *International Journal of Refractory Metals and Hard Materials*, 2020, 93: 105357.
- [57] Q Liu, G Wang, X Sui, et al. Microstructure and mechanical properties of ultra-fine grained MoNbTaTiV refractory high-entropy alloy fabricated by spark plasma sintering. *Journal of Materials Science and Technology*, 2019, 35(11): 2600-2607.
- [58] J L Zhou, Y H Cheng, Y X Chen, et al. Composition design and preparation process of refractory high-entropy alloys: A review. *International Journal of Refractory Metals and Hard Materials*, 2022, 105: 105836.
- [59] J P Fang, Q Wang, J Cai, et al. Research on low-temperature bonding technology using metal nanoparticles prepared by magnetron sputtering. *Journal of Mechanical Engineering*, 2022, 58(2): 34-42. (in Chinese)
- [60] W H Kao, Y L Su, J H Horng, et al. Mechanical, tribological, anti-corrosion and anti-glass sticking properties of high-entropy TaNbSiZrCr carbide coatings prepared using radio-frequency magnetron sputtering. *Materials Chemistry and Physics*, 2021, 268: 124741.
- [61] P Hruška, F Lukáč, S Cichoň, et al. Oxidation of amorphous HfNbTaTiZr high entropy alloy thin films prepared by DC magnetron sputtering. *Journal of Alloys and Compounds*, 2021, 869: 157978.
- [62] R Chen, Z Cai, J Pu, et al. Effects of nitriding on the microstructure and properties of VAlTiCrMo high-entropy alloy coatings by sputtering technique. *Journal of Alloys and Compounds*, 2020, 827: 153836.
- [63] M Dehestani, S Sharafi, G R Khayati. The effect of pulse current density on the microstructure, magnetic, mechanical, and corrosion properties of high-entropy alloy coating Fe-Co-Ni-Mo-W, achieved through electro co-deposition. *Intermetallics*, 2022, 147: 107610.
- [64] Y Tao, H Q Wang, H Ke, et al. Microstructure and wear behavior of AlCrTiNbMo high-entropy alloy coating prepared by electron beam cladding on Ti600 substrate. *Vacuum*, 2022, 199: 110928.
- [65] N Li, W Liu, Y Wang, et al. Laser Additive manufacturing on metal matrix composites: a review. *Chinese Journal of Mechanical Engineering*, 2021, 34(1): 38-54.
- [66] Q Y Li, H Zhang, D C Li, et al. Manufacture of WNbMoTa high performance high-entropy alloy by laser additive manufacturing. *Journal of Mechanical Engineering*, 2019, 55(15): 10-16. (in Chinese)
- [67] A O Moghaddam, N A Shaburova, M N Samodurova, et al. Additive manufacturing of high entropy alloys: A practical review. *Journal of Materials Science and Technology*, 2021, 77: 131-162.
- [68] X Li. Additive manufacturing of advanced multi-component alloys: bulk metallic glasses and high entropy alloys. *Advanced Engineering Materials*, 2018, 20(5): 1700874.
- [69] Y Chew, G J Bi, Z G Zhu. Microstructure and enhanced strength of laser aided additive manufactured CoCrFeNiMn high entropy alloy. *Materials Science and Engineering: A*, 2019, 744: 137-144.
- [70] H Christian. Combining thermodynamic modeling and 3D printing of elemental powder blends for high-throughput investigation of high-entropy alloys-Towards rapid alloy screening and design. *Materials Science and Engineering: A*, 2017, 688(14): 180-189.
- [71] Q Li, H Zhang, D Li, et al. W,NbMoTa refractory high-entropy alloys fabricated by laser cladding deposition. *Materials*, 2019, 12(3): 533.
- [72] Y Brief, M Thomas, I Todd. The use of high-entropy alloys in additive manufacturing. *Scripta Materialia*, 2015, 99(1): 93-96.
- [73] H Zhang, Y Zhao, J Cai, et al. High-strength NbMoTaX refractory high-entropy alloy with low stacking fault energy eutectic phase via laser additive manufacturing. *Materials and Design*, 2021, 201: 109462.
- [74] H Dobbstein, E L Gurevich, E P George, et al. Laser metal deposition of compositionally graded TiZrNbTa refractory high-entropy alloys using elemental powder blends. *Additive Manufacturing*, 2019, 25: 252-262.
- [75] H Zhang, Y Zhao, S Huang, et al. Manufacturing and analysis of high-performance refractory high-entropy alloy via selective laser melting (SLM). *Materials*, 2019, 12(5): 720.
- [76] H Zhang, W Xu, Y Xu. The thermal-mechanical behavior of WTaMoNb high-entropy alloy via selective laser melting (SLM): Experiment and simulation. *International Journal of Advanced Manufacturing Technology*, 2018, 96: 461-474.
- [77] M Galati, L Iuliano. A literature review of powder-based electron beam melting focusing on numerical simulations. *Additive Manufacturing*, 2018, 19: 1-20.
- [78] T Fujieda, H Shiratori, K Kuwabarak. First demonstration of promising selective electron beam melting method for utilizing high entropy alloys as engineering materials. *Materials Letters*, 2015, 159: 12-15.
- [79] H Shiratori, T Fujieda, K Yamanakak. Relationship between the microstructure and mechanical properties of an equiatomic AlCoCrFeNi high

- entropy alloy fabricated by selective electron beam melting. *Materials Science and Engineering: A*, 2016, 656(22): 39-46.
- [80] J Chen, X Y Zhou, W L Wang, et al. A review on fundamental of high entropy alloys with promising high temperature properties. *Journal of Alloys and Compounds*, 2018, 760: 15-30.
- [81] S Lee, G Choi, K Lee. TRIP-assisted compressive ductility in Ti-rich $Ti_{60}Mo_{10}V_{10}Cr_{10}Zr_{10}$ refractory medium-entropy alloy. *International Journal of Refractory Metals and Hard Materials*, 2021, 100: 105628.
- [82] J Čížek, P Haušild, M Cieslar, et al. Strength enhancement of high entropy alloy HfNbTaTiZr by severe plastic deformation. *Journal of Alloys and Compounds*, 2018, 768: 924-937.
- [83] Y L Guo, J Y He, Z M Li, et al. Strengthening and dynamic recrystallization mediated by Si-alloying in a refractory high entropy alloy. *Materials Science and Engineering A*, 2022, 832: 142480.
- [84] R R Eleti, T Bhattacharjee, A Shibata, et al. Unique deformation behavior and microstructure evolution in high temperature processing of HfNbTaTiZr refractory high entropy alloy. *Acta Materialia*, 2019, 171: 132-145.
- [85] Y C Huang, Y C Lai, Y H Lin, et al. A study on the severely cold-rolled and annealed quaternary equiatomic derivatives from quinary HfNbTaTiZr refractory high entropy alloy. *Journal of Alloys and Compounds*, 2021, 855: 157404.
- [86] Y K Cao, Y Liu, Y P Li, et al. Precipitation behavior and mechanical properties of a hot-worked $TiNbTa_{0.5}ZrAl_{0.5}$ refractory high entropy alloy. *International Journal of Refractory Metals and Hard Materials*, 2020, 86: 105132.
- [87] N D Stepanova, N Y Yurchenko, A O Gridneva, et al. Structure and hardness of B2 ordered refractory $AlNbTiVZr_{0.5}$ high entropy alloy after high-pressure torsion. *Materials Science and Engineering A*, 2018, 716: 308-315.
- [88] R R Eleti, A H Chokshi, A Shibata, et al. Unique high-temperature deformation dominated by grain boundary sliding in heterogeneous necklace structure formed by dynamic recrystallization in HfNbTaTiZr BCC refractory high entropy alloy. *Acta Materialia*, 2020, 183: 64-77.
- [89] F Y Dong, Y Yuan, W D Li, et al. Hot deformation behavior and processing maps of an equiatomic $MoNbHfZrTi$ refractory high entropy alloy. *Intermetallics*, 2020, 126: 106921.
- [90] Q Liu, G F Wang, Y K Liu, et al. Hot deformation behaviors of an ultrafine-grained $MoNbTaTiV$ refractory high-entropy alloy fabricated by powder metallurgy. *Materials Science and Engineering A*, 2021, 809: 140922.
- [91] T Q Cao, W Q Guo, W Lu, et al. Strain rate dependent deformation behavior of BCC-structured $Ti_{29}Zr_{24}Nb_{23}Hf_{24}$ high entropy alloy at elevated temperatures. *Journal of Alloys and Compounds*, 2021, 891: 161859.
- [92] O N Senkov, S L Semiatin. Microstructure and properties of a refractory high-entropy alloy after cold working. *Journal of Alloys and Compounds*, 2015, 649(15): 1110-1123.
- [93] R R Eleti, V Raju, M Veerasham, et al. Influence of strain on the formation of cold-rolling and grain growth textures of an equiatomic HfZrTiTaNb refractory high entropy alloy. *Materials Characterization*, 2018, 136: 286-292.
- [94] N Y Yurchenko, E S Panina, S V Zherebtsov, et al. Microstructure evolution of a novel low-density Ti-Cr-Nb-V refractory high entropy alloy during cold rolling and subsequent annealing. *Materials Characterization*, 2019, 158: 109980.
- [95] W Wu, S Ni, Y Liu, et al. Effects of cold rolling and subsequent annealing on the microstructure of a HfNbTaTiZr high-entropy alloy. *Journal of Materials Research*, 2016, 31: 3815-3823.
- [96] S W McAlpine, J V Logan, M P Short. Predicting single phase stability and segregation in the NbMoTaTi-(W, V) high entropy alloy system with the vacancy exchange potential. *Scripta Materialia*, 2021, 191: 29-33.
- [97] C Lee, G Song, M C Gao, et al. Lattice distortion in a strong and ductile refractory high-entropy alloy. *Acta Materialia*, 2018, 160: 158-172.
- [98] N Yurchenko, E Panina, M Tikhonovsky, et al. A new refractory Ti-Nb-Hf-Al high entropy alloy strengthened by orthorhombic phase particles. *International Journal of Refractory Metals and Hard Materials*, 2020, 92, 105322.
- [99] N D Stepanov, N Y Yurchenko, D G Shaysultanov, et al. Effect of Al on structure and mechanical properties of $Al_xNbTiVZr$ ($x = 0, 0.5, 1, 1.5$) high entropy alloys. *Materials Science and Technology*, 2015, 31(10): 1184-1193.
- [100] V Soni, O N Senkov, J-P Couzinié, et al. Phase stability and microstructure evolution in a ductile refractory high entropy alloy $Al_{10}Nb_{15}Ta_5Ti_{30}Zr_{40}$. *Materialia*, 2020, 9: 100569.
- [101] C C Juan, M H Tsai, C W Tsai, et al. Simultaneously increasing the strength and ductility of a refractory high-entropy alloy via grain refining. *Materials Letters*, 2016, 184: 200-203.
- [102] Q Wang, J C Han, Y F Liu, et al. Coherent precipitation and stability of cuboidal nanoparticles in body-centered-cubic $Al_{0.4}Nb_{0.5}Ta_{0.5}TiZr_{0.8}$ refractory high entropy alloy. *Scripta Materialia*, 2021, 190: 40-45.
- [103] V Soni, B Gwalani, T Alam, et al. Phase inversion in a two-phase, BCC+B2, refractory high entropy alloy. *Acta Materialia*, 2020, 185: 89-97.
- [104] J Q Yao, X W Liu, N Gao, et al. Phase stability of a ductile single-phase BCC Hf_{0.5}Nb_{0.5}Ta_{0.5}Ti_{1.5}Zr refractory high-entropy alloy. *Intermetallics*, 2018, 98: 79-88.
- [105] C H Tu, S-K Wu, L Chieh. A study on severely cold-rolled and intermediate temperature aged HfNbTiZr refractory high-entropy alloy. *Intermetallics*, 2020, 126: 106935.
- [106] R Feng, M C Gao, C Zhang, et al. Phase stability and transformation in a light-weight high entropy alloy. *Acta Materialia*, 2018, 146: 280-293.
- [107] R Feng, C Zhang, M C Gao, et al. High-throughput design of high-performance lightweight high-entropy alloys. *Nature Communications*, 2021, 12(1): 4329.
- [108] J M Rickman, H M Chan, M P Harmer, et al. Materials informatics for the screening of multi-principal elements and high-entropy alloys. *Nature Communications*, 2019, 10: 2618.
- [109] F G Coury, K D Clarke, C S Kiminami, et al. High throughput discovery and design of strong multicomponent metallic solid solutions. *Science Reports*, 2018, 8: 8600.
- [110] S M Shaikh, V S Hariharan, S K Yadav, et al. CALPHAD and rule-of-mixtures: a comparative study for refractory high entropy alloys. *Intermetallics*, 2020, 127: 106926.
- [111] O N Senkov, S Gorsse, D B Miracle. High temperature strength of refractory complex concentrated alloys. *Acta Materialia*, 2019, 175(15): 394-405.
- [112] H W Yao, J W Qiao, J A Hawkb, et al. Mechanical properties of refractory high-entropy alloys: Experiments and modeling. *Journal of Alloys and Compounds*, 2017, 696(5): 1139-1150.
- [113] Y Gao, L J Qiao, D T Wu, et al. First principle calculation of the effect of Cr, Ti content on the properties of $VMoNbTaW_x$ ($M=Cr, Ti$) refractory high entropy alloy. *Vacuum*, 2020, 179: 10945.
- [114] Y L Hu, L H Bai, Y G Tong, et al. First-principle calculation investigation of NbMoTaW based refractory high entropy alloys. *Journal of Alloys and Compounds*, 2020, 827: 153963.
- [115] Y Zhang, T T Zuo, Z Tang, et al. Microstructures and properties of high-entropy alloys. *Progress in Materials Science*, 2014, 61: 1-93.
- [116] S S Sohn, A K D Silva, Y Ikeda, et al. Ultrastrong medium-entropy single-phase alloys designed via severe lattice distortion. *Advanced Materials*, 2019, 31: 1807142.
- [117] E Ma. Unusual dislocation behavior in high-entropy alloys. *Scripta Materialia*, 2020, 181: 127-133.
- [118] Y Gao, L Qiao, D Wu, et al. First principle calculation of the effect of Cr, Ti content on the properties of $VMoNbTaW_x$ ($M=Cr, Ti$) refractory high entropy alloy. *Vacuum*, 2020, 179: 109459.
- [119] C M Liu, H M Wang, S Q Zhang, et al. Microstructure and oxidation behavior of new refractory high entropy alloys. *Journal of Alloys and Compounds*, 2014, 583: 162-169.
- [120] P Zhang, Y Li, Z Chen, et al. Oxidation response of a vacuum arc melted NbZrTiCrAl refractory high entropy alloy at 800-1200 degrees C. *Vacuum*, 2019, 162: 20-27.
- [121] W Li, P K Liaw, Y Gao. Fracture resistance of high entropy alloys: a review. *Intermetallics* 2018, 99: 69-83.
- [122] W Liu, N Li, Biao Zhou, et al. Progress in additive manufacturing on complex structures and high-performance materials. *Journal of Mechanical Engineering*, 2019, 55(20): 128-151. (in Chinese).
- [123] N Li, S Huang, G D Zhang, et al. Progress in additive manufacturing on new materials: A review. *Journal of Materials Science and Technology*, 2019, 35: 242-269.